

## A Smooth Solvation Potential Based on the Conductor-Like Screening Model

Darrin M. York<sup>\*,†</sup> and Martin Karplus<sup>\*</sup>

Laboratoire de Chimie Biophysique, Institut Le Bel, Université Louis Pasteur, 4 rue Blaise Pascal, 67000 Strasbourg, France, and Department of Chemistry and Chemical Biology, Harvard University, Cambridge, Massachusetts 02138

Received: June 23, 1999

The development of a smooth solvation potential from which analytic derivatives can be derived is important for molecular applications that require geometry optimization and conformational sampling. Derivatives in conventional boundary element solvation methods are typically treated approximately, and contain singularities that arise from discontinuities in the potential. We present a simple smooth solvation potential that is based on the conductor-like screening model proposed by Klamt and Schüürmann (Klamt, A.; Schüürmann, G. J. *Chem. Soc., Perkin. Trans. 2*, **1993**, 799). The model uses a simple solvent accessible surface with an atomic sphere discretization based on high-order angular quadrature schemes for spherical harmonics. Surface elements are modeled by spherical Gaussian functions with exponents calibrated to obtain the exact Born ion energy and uniform surface charge density and to avoid Coulomb singularities present in conventional point-charge surface element models. The set of linear equations are modified to produce a *rigorously smooth* solvation potential by allowing the effect of new surface elements to be turned on or off over a finite switching region around each atom. Numerical tests of the method are provided, in addition to discussions of rotational variance, generalization to arbitrary internal dielectric, use of constraints, and extension to a smooth surface area model.

### 1. Introduction

Solvation has a profound effect on the behavior of biomolecules.<sup>1–3</sup> Theoretical treatments of solvation<sup>4</sup> range in complexity from explicit simulation of many solvent molecules to implicit models that provide an approximate mean field picture of the bulk solvent. The spectrum of methods that have evolved and that are routinely applied involve a balance of accuracy and computational effort. Explicit simulation of the solvent environment provides a detailed description of solvation. However, this type of treatment is very costly and frequently requires a high degree of configurational sampling to determine equilibrium properties. Implicit models based on a dielectric continuum approximation are orders of magnitude more efficient. However, they usually provide less accuracy and do not give explicit dynamical information about the solvent degrees of freedom. Integral equation theories offer an alternative that helps bridge the gap between explicit solvent simulations and simple continuum treatments of solvation.<sup>5</sup> In certain cases, hybrid methods that combine a hierarchy of theoretical levels may be the best compromise between reliability and computational feasibility.

There are many instances where simple continuum solvation models are useful.<sup>6–8</sup> For problems that involve very large molecules or require many evaluation of the solvation energy, alternative higher level approaches are not tractable. Continuum solvation models have been particularly useful for the calculation of electrostatic fields and solvation free energies of large biomolecules,<sup>1,2,4</sup> titration curves, and pK<sub>a</sub> shifts in proteins,<sup>1,2,9,10</sup> solvation effects in quantum mechanical calculations,<sup>7,8</sup> non-equilibrium solvation energies,<sup>11</sup> and the stability of peptides and proteins in molecular simulations of folding events.<sup>12,13</sup>

For a solvation model to be useful in calculations such as geometry optimization, transition state searches, and molecular dynamics simulations, it must yield a potential with continuous first derivatives with respect to the nuclear positions. In what follows, the term “smooth” is used to describe such a potential.<sup>5,6</sup> These conditions are not rigorously fulfilled in most boundary element methods due to the difficulty in defining an analytic functional form for the surface elements from which gradients can be derived. The literature is often misleading in claiming derivation of analytic derivatives of solvation potentials when, in fact, the solvation potentials contain discontinuities that cause gradients to become singular. The most common instance of this involves the neglect of derivatives with respect to the area of individual surface elements that leads to the so-called “fixed cavity” approximation. Expressions have been derived for surface element derivatives for given *tessellation* of the molecular surface that improves the smoothness of the potential.<sup>14</sup> However, the singularity problem persists if the tessellation procedure itself is not a smooth function of the atomic coordinates (which is typically the case). Moreover, other difficulties can arise such as Coulomb singularities in methods that model surface elements by point charges,<sup>6,15,16</sup> and the neglect of derivatives with respect to scaling factors that enforce surface charge normalization in accord with Gauss’ law.<sup>17,18</sup>

In this paper, an analytic solvation potential based on the conductor-like screening model<sup>15</sup> is introduced that has the advantages that it (i) is a smooth analytic function of the atomic positions, (ii) uses a simple solvent accessible surface, (iii) uses surface discretization based on angular quadrature rules, (iv) avoids point-charge singularities with a Gaussian surface element model, and (v) is calibrated to obtain the exact Born energy for spherical ions. The first section outlines the relevant

<sup>†</sup> Present address: Department of Chemistry, University of Minnesota, Minneapolis, MN 55455.

electrostatic theory and presents variational relations used for solving numerical electrostatic problems of the type considered here. The second section describes the conductor-like screening model and presents the new approach. The third section provides numerical tests of the accuracy and convergence of the model. The appendices contain several useful extensions and generalizations of the theory and methods.

## 2. Theory

**2.1. Electrostatics.** The electrostatic potential  $\phi_0$  due to a fixed charge distribution  $\rho_0$  in the absence of a dielectric medium is a solution of the Poisson equation in free space

$$\nabla^2 \phi_0 = -4\pi \rho_0 \quad (1)$$

The Green's function solution for the potential can be written as

$$\phi_0(\mathbf{r}) = \int G_0(\mathbf{r}, \mathbf{r}') \rho_0(\mathbf{r}') d^3 r' \quad (2)$$

where  $G_0(\mathbf{r}, \mathbf{r}')$  satisfies the differential equation

$$\nabla_{\mathbf{r}}^2 G_0(\mathbf{r}, \mathbf{r}') = -4\pi \delta(\mathbf{r} - \mathbf{r}') \quad (3)$$

and depends on the boundary conditions of the problem; e.g.,

$$G_0(\mathbf{r}, \mathbf{r}') = \begin{cases} \frac{1}{|\mathbf{r} - \mathbf{r}'|} & \text{for nonperiodic systems} \\ \frac{4\pi}{V} \sum_{\mathbf{k} \neq 0} \frac{e^{i\mathbf{k} \cdot (\mathbf{r} - \mathbf{r}')}}{k^2} & \text{for periodic systems} \end{cases} \quad (4)$$

where  $V$  is the volume of the periodic cell,  $\mathbf{k} = 2\pi\mathbf{m}$ , and  $\mathbf{m} = m_1\mathbf{a}_1^* + m_2\mathbf{a}_2^* + m_3\mathbf{a}_3^*$  where  $(\mathbf{a}_1^*, \mathbf{a}_2^*, \mathbf{a}_3^*)$  are the reciprocal space lattice vectors and  $(m_1, m_2, m_3)$  are integers. Henceforth the nonperiodic case is considered explicitly with the understanding that extension to periodic systems can be realized by modification of the Green's function.

In the absence of a polarization response, the electrostatic potential of eq 2 is

$$\phi_0(\mathbf{r}) = \int \frac{\rho_0(\mathbf{r}')}{|\mathbf{r} - \mathbf{r}'|} d^3 r' \quad (5)$$

If in addition to  $\rho_0$  there is an *electric dipole polarization*  $\mathbf{P}$  (it is indicated below how  $\mathbf{P}$  arises), the resulting potential is given by<sup>19</sup>

$$\begin{aligned} \phi(\mathbf{r}) &= \int \left( \frac{\rho_0(\mathbf{r}')}{|\mathbf{r} - \mathbf{r}'|} + \frac{\mathbf{P}(\mathbf{r}') \cdot (\mathbf{r} - \mathbf{r}')}{|\mathbf{r} - \mathbf{r}'|^3} \right) d^3 r' \\ &= \int \left( \frac{\rho_0(\mathbf{r}')}{|\mathbf{r} - \mathbf{r}'|} + \mathbf{P}(\mathbf{r}') \cdot \nabla_{\mathbf{r}'} \left( \frac{1}{|\mathbf{r} - \mathbf{r}'|} \right) \right) d^3 r' \\ &= \int \left( \frac{\rho_0(\mathbf{r}') - \nabla \cdot \mathbf{P}(\mathbf{r}')}{|\mathbf{r} - \mathbf{r}'|} \right) d^3 r' \end{aligned} \quad (6)$$

Operating on both sides of eq 6 with the Laplacian gives

$$\nabla^2 \phi = -\nabla \cdot \mathbf{E} = -4\pi [\rho_0 - \nabla \cdot \mathbf{P}] = -4\pi [\rho_0 + \sigma_{\text{pol}}] \quad (7)$$

where  $\sigma_{\text{pol}} = -\nabla \cdot \mathbf{P}$  is the *dipole polarization density* and  $\mathbf{E} = -\nabla \phi$  is the *electric field*. The *electric displacement*  $\mathbf{D}$  (consider-

ing only dipole polarization terms from the medium) is defined by

$$\mathbf{D} = \mathbf{E} + 4\pi\mathbf{P} \quad (8)$$

which leads to the Maxwell relation

$$\nabla \cdot \mathbf{D} = 4\pi \rho_0 \quad (9)$$

In the case that the electric polarization arises as a linear isotropic response to the total electric field,

$$\mathbf{P} = \chi_e \cdot \mathbf{E} \quad (10)$$

where  $\chi_e$  is the *electric susceptibility* of the medium (in the case of an anisotropic medium this quantity is a tensor). Substitution of eq 10 into eq 8 gives

$$\mathbf{D} = (1 + 4\pi\chi_e)\mathbf{E} = \epsilon\mathbf{E} \quad (11)$$

where the definition of the *static dielectric function*,  $\epsilon = (1 + 4\pi\chi_e)$ , has been introduced. This leads to the familiar Poisson equation for a linear isotropic polarizable medium

$$\nabla \cdot (\epsilon \nabla \phi) = -4\pi \rho_0 \quad (12)$$

If the potential is divided into static and polarization components  $\phi = \phi_0 + \phi_{\text{pol}}$ , where  $\phi_0$  satisfies the Poisson equation in free space (eq 1), eq 12 leads to a differential equation relating the polarization density and potential,

$$\nabla^2 \phi_{\text{pol}} = -4\pi \rho_0 \frac{1 - \epsilon}{\epsilon} - \frac{\nabla \epsilon}{\epsilon} \cdot \nabla \phi = -4\pi \sigma_{\text{pol}} \quad (13)$$

Equation 13 is a general equation for the polarization density  $\sigma_{\text{pol}}$ , which is not necessarily a surface charge density. Integration of  $\sigma_{\text{pol}}$  over all space leads to Gauss' law

$$\begin{aligned} \int \sigma_{\text{pol}} d^3 r &= \int \rho_0 \left( \frac{1 - \epsilon}{\epsilon} \right) d^3 r + \frac{1}{4\pi} \int \frac{\nabla \epsilon}{\epsilon} \cdot \nabla \phi d^3 r \\ &= \int \rho_0 \left( \frac{1}{\epsilon} - 1 \right) d^3 r + \frac{1}{4\pi} \int \nabla \left( \frac{1}{\epsilon} \right) \cdot \epsilon \mathbf{E} d^3 r \\ &= \int \rho_0 \left( \frac{1}{\epsilon} - 1 \right) d^3 r - \frac{1}{4\pi} \int \left( \frac{1}{\epsilon} \right) \nabla \cdot \mathbf{D} d^3 r + \\ &\quad \frac{1}{4\pi} \int_{S=\infty} \left( \frac{1}{\epsilon} \right) \mathbf{D} \cdot \mathbf{n} da \\ &= - \int \rho_0 d^3 r + \frac{1}{4\pi} \int_{S=\infty} \left( \frac{1}{\epsilon} \right) \mathbf{D} \cdot \mathbf{n} da \\ &= - \left( \frac{\epsilon_2 - 1}{\epsilon_2} \right) \int \rho_0 d^3 r \end{aligned} \quad (14)$$

where in the last equality it has been assumed that the dielectric function has a constant value  $\epsilon_2$  at infinity (for a nonperiodic system). Equations 13 and 14 form the basis of the method presented in section 3.2. The remainder of this subsection focuses on how the standard boundary element equations,<sup>6</sup> which differ from those of the present work, are derived from eq 13 with certain assumptions.

For a static charge density  $\rho_0$  that is completely contained in a closed cavity with unit dielectric; i.e.,  $\rho_0 = 0$  everywhere  $\epsilon \neq 1$ , eq 13, reduces to

$$\sigma_{\text{pol}} = \frac{1}{4\pi} \frac{\nabla \epsilon}{\epsilon} \cdot \nabla \phi = - \frac{1}{4\pi} \nabla \ln(\epsilon) \cdot \mathbf{E} \quad (15)$$

In this situation  $\sigma_{\text{pol}}$  is nonzero only in regions where  $\epsilon$  is varying (e.g., at a dielectric boundary where  $\nabla \ln(\epsilon) \neq 0$ ). Equations 13 and 15 can be used to solve for  $\sigma_{\text{pol}}$  if  $\nabla \ln(\epsilon)$  is finite. If  $\nabla \ln(\epsilon)$  is *not* finite, as in the case of a cavity of constant internal dielectric ( $\epsilon_1$  in  $V_1$ ) that changes discontinuously to a bulk value ( $\epsilon_2$  in  $V_2$  outside of  $V_1$ ) at the boundary surface, care must be taken to ensure the boundary conditions:

$$(\mathbf{D}_2 - \mathbf{D}_1) \cdot \mathbf{n}_{21} = 4\pi\sigma_0 \quad (16)$$

$$(\mathbf{E}_2 - \mathbf{E}_1) \times \mathbf{n}_{21} = 0 \quad (17)$$

where  $\mathbf{n}_{21}$  is the outward unit normal vector pointing from region 1 to region 2, and  $\sigma_0$  is the *static surface charge density* at the dielectric boundary (not the induced polarization surface charge density  $\sigma_{\text{pol}}$ ), and is normally taken to be zero. The discontinuity of the dielectric under the boundary conditions of eqs 16 and 17 results in a polarization surface charge density (see Appendix A)

$$\sigma_{\text{pol}} = -(\mathbf{P}_2 - \mathbf{P}_1) \cdot \mathbf{n}_{21} \quad (18)$$

where  $\mathbf{P}_i$  is given by

$$\mathbf{P}_i = \left( \frac{\epsilon_i - 1}{4\pi} \right) \mathbf{E}_i = \left( \frac{\epsilon_i - 1}{4\pi\epsilon_i} \right) \mathbf{D}_i \quad (19)$$

Most boundary elements methods recast eqs 18 and 19 into a set of linear algebraic equations that are solved to give the polarization surface charge vector  $\sigma_{\text{pol}}$ .<sup>6</sup> The assumptions inherent in the standard formulation of these methods are that (1) the charge density is completely contained inside a cavity of dielectric  $\epsilon_1 = 1$  (leading to eq 15), 2) the dielectric changes abruptly to the external value  $\epsilon_2$  at the cavity surface (leading to eqs 18 and 19), and (3) no static surface charge is considered ( $\sigma_0 = 0$ ).

Substitution of eq 19 into eq 18 under the boundary conditions of eqs 16 and 17 (with  $\sigma_0 = 0$ ) leads to expressions for the polarization charge density in terms of the dielectric displacement,

$$\sigma_{\text{pol}} = -\frac{1}{4\pi} \left( \frac{\epsilon_2 - \epsilon_1}{\epsilon_1\epsilon_2} \right) \mathbf{D} \cdot \mathbf{n}_{21} \quad (20)$$

In this case, Gauss' law for the total polarization *surface charge* (the component of the polarization density *on the cavity surface*) is

$$\begin{aligned} \int_S \sigma_{\text{pol}} \, da &= -\frac{1}{4\pi} \int_S \left( \frac{\epsilon_2 - \epsilon_1}{\epsilon_1\epsilon_2} \right) \mathbf{D} \cdot \mathbf{n}_{21} \, da \\ &= -\frac{1}{4\pi} \left( \frac{\epsilon_2 - \epsilon_1}{\epsilon_1\epsilon_2} \right) \int_{V_1} \nabla \cdot \mathbf{D} \, d^3r \\ &= -\left( \frac{\epsilon_2 - \epsilon_1}{\epsilon_1\epsilon_2} \right) \int_{V_1} \rho_0 \, d^3r \\ &= -\left( \frac{\epsilon_2 - \epsilon_1}{\epsilon_1\epsilon_2} \right) Q_0(V_1) \end{aligned} \quad (21)$$

where  $Q_0(V_1)$  is the integrated charge associated with  $\rho_0$  inside  $V_1$ . For the case of a cavity of dielectric  $\epsilon_1$  surrounded by a conducting medium ( $\epsilon_2 = \infty$ ), the total surface charge is  $-Q_0(V_1)/\epsilon_1$ . Note that eq 21 involves integration *over the cavity surface* whereas eq 14 involves integration *over all space*.

Equation 21 is equivalent to eq 14 in the case that  $\epsilon_1 = 1$ , and  $Q_0(V_1) = \int \rho_0 \, d^3r$  integrated over all space (i.e.,  $\rho_0$  is completely contained in  $V_1$ ), in which case from eqs 13 and 15 it can be seen that  $\sigma_{\text{pol}}$  resides only on the cavity surface. The distinction between eqs 21 and 14 becomes important in numerical calculations that use constraints on the total surface charge and in consideration of the generalized model presented in section 3.1.

The strategy of determining  $\phi_{\text{pol}}$  directly from  $\sigma_{\text{pol}}$  via eqs 5 and 18–20 is complicated by the fact that  $\sigma_{\text{pol}}$  itself depends on  $\phi_{\text{pol}}$  via the electric field; hence, solution of the equations typically requires an iterative procedure or matrix inversion process.<sup>16</sup>

**2.2. Variational Principles.** In this section several variational principles are presented that can be used with standard optimization techniques to solve multidimensional integral–differential equations that occur in electrostatic problems. In particular, the variational principle for the solvation models presented in the next section are derived. For a review of the calculus of variations, see ref 20.

The general expression for the electrostatic energy of a charge density in a (nonlinear) dielectric medium is<sup>19</sup>

$$W = \frac{1}{4\pi} \int d^3r \int_0^{\mathbf{D}} \mathbf{E} \cdot \delta \mathbf{D} \quad (22)$$

If the response of the medium is linear, then

$$\int_0^{\mathbf{D}} \mathbf{E} \cdot \delta \mathbf{D} = \frac{1}{2} \mathbf{E} \cdot \mathbf{D} \quad (23)$$

and the electrostatic energy takes the simplified form

$$W = \frac{1}{8\pi} \int \mathbf{E} \cdot \mathbf{D} \, d^3r = \frac{1}{2} \int \rho_0 \phi \, d^3r \quad (24)$$

For a linear isotropic polarizable medium with  $\mathbf{D} = \epsilon \mathbf{E} = -\epsilon \nabla \phi$ , one can construct the functional

$$W_\phi[\phi; \rho_0, \epsilon] = \int \rho_0 \phi \, d^3r - \frac{1}{8\pi} \int \nabla \phi \cdot \epsilon \cdot \nabla \phi \, d^3r \quad (25)$$

where  $\rho_0$  and  $\epsilon$  are functional parameters. The condition that the functional of eq 25 is stationary with respect to variations in  $\phi$  is

$$\frac{\delta W_\phi[\phi; \rho_0, \epsilon]}{\delta \phi(\mathbf{r})} = \rho_0(\mathbf{r}) + \frac{1}{4\pi} \nabla \cdot [\epsilon(\mathbf{r}) \nabla \phi(\mathbf{r})] = 0 \quad (26)$$

and is equivalent to the Poisson differential equation (eq 12). The second functional variation is given by

$$\frac{\delta^2 W_\phi[\phi; \rho_0, \epsilon]}{\delta \phi(\mathbf{r}) \delta \phi(\mathbf{r}')} = \frac{1}{4\pi} \nabla_{\mathbf{r}} \cdot [\epsilon(\mathbf{r}') \nabla_{\mathbf{r}} \delta(\mathbf{r} - \mathbf{r}')] \quad (27)$$

This operator is negative for  $\epsilon > 0$ , since for any function  $f$  that obeys the boundary conditions of the problem,

$$\begin{aligned} \int \int f(\mathbf{r}) \nabla_{\mathbf{r}} \cdot [\epsilon(\mathbf{r}') \nabla_{\mathbf{r}} \delta(\mathbf{r} - \mathbf{r}')] f(\mathbf{r}') \, d^3r \, d^3r' &= \\ - \int \int f(\mathbf{r}) [\epsilon(\mathbf{r}') \nabla_{\mathbf{r}} \delta(\mathbf{r} - \mathbf{r}')] \nabla f(\mathbf{r}') \, d^3r \, d^3r' &= \\ - \int \epsilon(\mathbf{r}) |\nabla f(\mathbf{r})|^2 \, d^3r &\leq 0 \end{aligned} \quad (28)$$

The functional  $W[\phi; \rho_0, \epsilon < 0]$  is said to be *concave* with respect to  $\phi$  and is a *maximum* at the stationary point. For  $\epsilon = 1$ , the

functional is

$$W_\phi[\phi; \rho_0, \epsilon = 1] = \int \rho_0 \phi \, d^3r - \frac{1}{8\pi} \int \nabla \phi \cdot \nabla \phi \, d^3r = \int \rho_0 \phi \, d^3r + \frac{1}{8\pi} \int \phi \nabla^2 \phi \, d^3r \quad (29)$$

and the extremal condition  $\delta W_\phi / \delta \phi = 0$  leads to the Poisson equation in free space (eq 1). This is equivalent to the condition of *minimizing* the functional

$$\chi_E^2[\phi; \phi_0, \epsilon = 1] = \frac{1}{2} \int (\nabla \phi - \nabla \phi_0)^2 \, d^3r = \frac{1}{2} \int (\mathbf{E} - \mathbf{E}_0)^2 \, d^3r \quad (30)$$

where the  $\chi_E^2$  notation reflects the analogy to the  $\chi^2$  function that is minimized in least-square fitting procedures. As will be discussed later, eq 29 and 30 can be used to variationally expand densities (or potentials) in an auxiliary basis to solve electrostatic problems. The functional of eq 30 is a specific case of the more general functional

$$\begin{aligned} \chi_E^2[\phi; \phi_0, \epsilon] &= \frac{1}{2} \int [\epsilon^{1/2} \mathbf{E} - \epsilon^{-1/2} \mathbf{E}_0]^2 \, d^3r \\ &= \frac{1}{2} \int [\epsilon^{1/2} (\mathbf{E} - \epsilon^{-1} \mathbf{E}_0)]^2 \, d^3r \\ &= \frac{1}{2} \int \epsilon (\mathbf{E} - \epsilon^{-1} \mathbf{E}_0)^2 \, d^3r \end{aligned} \quad (31)$$

that has a stationary point equivalent to that of eqs 12 and 26. Note that in the above equations the unconstrained variational parameter is the scalar potential  $\phi$ , not the vector field  $\mathbf{E} = -\nabla \phi$ . Variation of the field would require the additional constraint  $\nabla \times \mathbf{E} = 0$  to ensure  $\mathbf{E}$  corresponds to minus the gradient of a scalar potential.

It is useful to transform the above functionals into ones that involve variations in the polarization potential  $\phi_{\text{pol}}$ . Let  $\phi = \phi_0 + \phi_{\text{pol}}$ , then

$$\begin{aligned} W_{\phi_{\text{pol}}}[\phi_{\text{pol}}; \rho_0, \epsilon] &= \int \left[ \rho_0 (1 - \epsilon) + \frac{\nabla \epsilon \cdot \nabla \phi_0}{4\pi} \right] \times \phi_{\text{pol}} \, d^3r \\ &- \frac{1}{8\pi} \int \nabla \phi_{\text{pol}} \cdot \epsilon \cdot \nabla \phi_{\text{pol}} \, d^3r - \frac{1}{8\pi} \int \nabla \phi_0 \cdot \epsilon \cdot \nabla \phi_0 \, d^3r \end{aligned} \quad (32)$$

$$\begin{aligned} \chi_{E_{\text{pol}}}^2[\phi_{\text{pol}}; \phi_0, \epsilon] &= \frac{1}{2} \int \epsilon (\mathbf{E}_0 + \mathbf{E}_{\text{pol}} - \epsilon^{-1} \mathbf{E}_0)^2 \, d^3r \\ &= \frac{1}{2} \int \epsilon \left[ \mathbf{E}_{\text{pol}} + \left( \frac{\epsilon - 1}{\epsilon} \right) \mathbf{E}_0 \right]^2 \, d^3r \end{aligned} \quad (33)$$

The variational conditions  $\delta W_{\phi_{\text{pol}}} / \delta \phi_{\text{pol}} = 0$  and  $\delta \chi_{E_{\text{pol}}}^2 / \delta \phi_{\text{pol}} = 0$  are equivalent to eq 13 for the polarization density. The effect of minimizing  $\chi_{E_{\text{pol}}}^2$  is analogous to a weighted least-squares fit of the polarization field with the scaled field  $-[(\epsilon - 1)/\epsilon] \mathbf{E}_0$  and weight factor  $\epsilon$ . It is clear that for  $\epsilon = 1$  there is no polarization field, and in the limit  $\epsilon = \infty$ ,  $\mathbf{E}_{\text{pol}}$  and  $\mathbf{E}_0$  must cancel. The advantage in working with this equation is that the polarization response can be obtained directly. In numerical finite difference solutions of the Poisson equation, frequently two calculations are employed to obtain the polarization energy ( $\phi$  and  $\phi_0$ ). Recently it has been proposed to apply the finite difference method directly to the equation for the

polarization potential and avoid calculation of  $\phi_0$  and the associated "self energy".<sup>21</sup> In most boundary element methods, including the present method, the polarization surface charge is solved for directly.

Consider the specific case of a cavity of  $\epsilon_1 = 1$  surrounded by a conductor  $\epsilon_2 = \infty$ . From eq 33,  $\phi_{\text{pol}}$  can be obtained by minimizing the quantity  $(\mathbf{E}_{\text{pol}} + \mathbf{E}_0)^2$  outside the cavity and can be achieved without approximation by constraining the variation of the polarization density to be on the surface of the cavity (at the dielectric boundary) *if the charge density is completely contained within the cavity*, as seen by eq 15. However, least-squares minimization of the difference of two electric fields in eq 30 gives the same stationary condition as maximization of the functional of eq 29. Hence, a solution for a conductor can be obtained through maximization of the functional  $W_\phi[\phi_{\text{pol}}; -\rho_0, \epsilon = 1]$  with respect to  $\phi_{\text{pol}}$  under the *constraint* that the polarization density occurs only at the cavity surface. The resulting functional is simply minus the *electrostatic interaction energy* of the polarization surface charge  $\sigma_{\text{pol}}$  with the static charge density  $\rho_0$  plus the *electrostatic self energy* of the former. Hence, the conductor surface charge density can be derived from minimization of the total electrostatic energy with respect to variations of the polarization density on the surface of the cavity. This forms the basic variational procedure for the conductor-like screening model.<sup>15</sup>

### 3. Solvation Models

In this section solvation models based on the electrostatic theory and variational principles presented in the previous section are developed. Discussion is restricted to the electrostatic component of the solvation energy. The so-called cavitation and dispersion terms<sup>6-8</sup> are not dealt with. The first subsection introduces the conductor-like screening model that forms the basis of the model proposed in the second subsection.

**3.1. The Conductor-Like Screening Model.** The conductor-like screening model was outlined in the original paper by Klamt and Schüürmann<sup>15</sup> and subsequently further developed and applied in quantum mechanical calculations.<sup>22-31</sup> A comprehensive discussion of this model follows, including generalization to arbitrary internal (solute) dielectric, constraint conditions (e.g., Gauss' law), and analytic gradient requirements.

*The Conventional Conductor-Like Screening Model.* The total electrostatic energy of a charge distribution contained in a cavity of unit dielectric surrounded by a conductor is given by

$$W = \frac{1}{2} \int \int (\sigma_{\text{pol}}(\mathbf{r}) + \rho_0(\mathbf{r})) G_0(\mathbf{r}, \mathbf{r}') (\sigma_{\text{pol}}(\mathbf{r}') + \rho_0(\mathbf{r}')) \, d^3r \, d^3r' = E_0 + E_{\text{pol}} \quad (34)$$

where

$$E_0 = \frac{1}{2} \int \int \rho_0(\mathbf{r}) G_0(\mathbf{r}, \mathbf{r}') \rho_0(\mathbf{r}') \, d^3r \, d^3r' \quad (35)$$

and

$$\begin{aligned} E_{\text{pol}} &= \frac{1}{2} \int \int \sigma_{\text{pol}}(\mathbf{r}) G_0(\mathbf{r}, \mathbf{r}') \sigma_{\text{pol}}(\mathbf{r}') \, d^3r \, d^3r' + \\ &\int \int \sigma_{\text{pol}}(\mathbf{r}) G_0(\mathbf{r}, \mathbf{r}') \rho_0(\mathbf{r}') \, d^3r \, d^3r' \end{aligned} \quad (36)$$

Here  $\sigma_{\text{pol}}$  is the induced reaction-field surface charge at the dielectric boundary, and  $G_0(\mathbf{r}, \mathbf{r}')$  is the appropriate Green's function (eq 4) of the Poisson equation in free space for the boundary conditions of the problem. The conductor surface

charge distribution  $\sigma_{\text{pol}}$  is a solution of the variational condition

$$\frac{\delta W}{\delta \sigma_{\text{pol}}(\mathbf{r})} = \frac{\delta E_{\text{pol}}}{\delta \sigma_{\text{pol}}(\mathbf{r})} = 0 \quad (37)$$

Thus, the conductor surface charge distribution minimizes the total electrostatic energy; i.e., there is no energetic penalty beyond the normal Coulomb self-energy of the surface charge associated with polarizing a conductor ( $\epsilon = \infty$ ). The particularly simple conductor variational condition is the basis of the conductor-like screening model. For a finite external dielectric  $\epsilon_2$ , the model scales the energy, gradient, and surface charge distribution by a factor  $f(\epsilon_2) = (\epsilon_2 - 1)/(\epsilon_2 + x)$  where  $x$  is a parameter between 0 and 2, chosen here to be 0 in accord with Gauss' law (eq 14). This introduces an error (relative to the exact solution of the dielectric problem) of the order  $(\epsilon_2^{-1})^{15}$  that is small for high dielectric media such as water ( $\epsilon_2 \approx 80$ ). Scaling the conductor surface charge is equivalent to minimization of a modified energy functional where the surface charge self-energy term of eq 34 is scaled by a factor  $1/f(\epsilon_2)$ . The factor  $f(\epsilon_2)$  insures that the polarization surface charge satisfies Gauss' law for an exact solution of the variational condition of eq 37 (this point is further addressed in the discussion of constraints). The differential equation that arises from eq 37 is transformed into an algebraic equation by the introduction of  $M$  basis functions for the representation of the surface charge  $\sigma_{\text{pol}}$  and  $N$  basis functions for the solute charge density  $\rho_0$

$$E_0 = \frac{1}{2} \rho_0^T \cdot \mathbf{C} \cdot \rho_0 = \frac{1}{2} \rho_0^T \cdot \phi_0 \quad (38)$$

$$E_{\text{pol}} = \frac{1}{f(\epsilon_2)} \frac{1}{2} \sigma_{\text{pol}}^T \cdot \mathbf{A}_0 \cdot \sigma_{\text{pol}} + \sigma_{\text{pol}}^T \cdot \mathbf{B} \cdot \rho_0 \\ = \frac{1}{2} \sigma_{\text{pol}}^T \cdot \mathbf{A} \cdot \sigma_{\text{pol}} + \sigma_{\text{pol}}^T \cdot \mathbf{B} \cdot \rho_0 \quad (39)$$

where  $\sigma_{\text{pol}}$  is an  $M \times 1$  vector containing the coefficients for the expansion of the polarization surface charge density,  $\rho_0$  is and  $N \times 1$  vector for expansion of the solute charge density,  $\phi_0 = \mathbf{C} \cdot \rho_0$  is the  $N \times 1$  static potential vector, and  $\mathbf{A}_0$ ,  $\mathbf{B}$ , and  $\mathbf{C}$  are  $M \times M$ ,  $M \times N$  and  $N \times N$  matrices, respectively, that define Coulomb interactions between the vectors, and  $\mathbf{A} = \mathbf{A}_0/f(\epsilon_2)$ . The variational condition is

$$\frac{\delta E_{\text{pol}}}{\delta \sigma_{\text{pol}}} = \mathbf{A} \cdot \sigma_{\text{pol}} + \mathbf{B} \cdot \rho_0 = 0 \quad (40)$$

and has solution

$$\sigma_{\text{pol}}^* = -\mathbf{A}^{-1} \cdot \mathbf{B} \cdot \rho_0 \quad (41)$$

where the superscript on  $\sigma_{\text{pol}}^*$  indicates the polarization surface charge that minimizes the energy. Substitution of eq 41 into eq 39 and addition of  $E_0$  in eq 38 leads to a compact solution in terms of the Green's function:

$$E = \frac{1}{2} \rho_0^T \cdot (\mathbf{C} - \mathbf{B}^T \cdot \mathbf{A}^{-1} \cdot \mathbf{B}) \cdot \rho_0 = \frac{1}{2} \rho_0^T \cdot \mathbf{G} \cdot \rho_0 \quad (42)$$

and

$$E_{\text{pol}} = \frac{1}{2} \rho_0^T \cdot (-\mathbf{B}^T \cdot \mathbf{A}^{-1} \cdot \mathbf{B}) \cdot \rho_0 = \frac{1}{2} \rho_0^T \cdot \mathbf{G}_{\text{pol}} \cdot \rho_0 \quad (43)$$

The above solution is particularly convenient for quantum mechanical calculations since the Green's function  $\mathbf{G} = \mathbf{G}_0 + \mathbf{G}_{\text{pol}} = \mathbf{C} - \mathbf{B}^T \cdot \mathbf{A}^{-1} \cdot \mathbf{B}$  can be computed once at the beginning of the self-consistent field (SCF) procedure where it enters as a modification to the Hamiltonian matrix elements. The calculation of the Green's function involves the inverse of the  $\mathbf{A}$  matrix that has dimensions  $M \times M$ , where  $M$  is the number of surface elements, and scales as  $O(M^3)$  as  $M$  becomes large. This is not a serious limitation for conventional quantum mechanical calculations that scale as the cube of the number of electrons (and hence system size) due to the orthonormality constraints on the molecular orbitals. The orthonormality conditions are typically enforced in the canonical Hartree–Fock and Kohn–Sham equations by solving a generalized eigenvalue/eigenvector problem at each iteration of the SCF procedure. Inversion of a symmetric positive definite matrix via, for example, a Cholesky decomposition, is much faster than diagonalization of a similar matrix of the same dimensions.<sup>32</sup> For very large systems, however, conventional quantum mechanical methods are not feasible, and it is necessary to employ “linear-scaling” electronic structure methods designed to circumvent the cubic scaling bottleneck of conventional methods (see ref 33 and references therein). In this case, the Green's function solution of eq 43 is also intractable, and one must devise methods that avoid construction and inversion of the full  $\mathbf{A}$  matrix. One such method utilizes a preconditioned conjugate gradient technique to directly minimize eq 39 with electrostatic interactions calculated using a linear-scaling recursive bisection multipole expansion method.<sup>26</sup>

*Generalization to Arbitrary Internal Dielectric.* The original conductor-like screening model considered the case of an internal unit dielectric. Here, the procedure is generalized to arbitrary internal dielectric  $\epsilon_1$ .

From eq 13, the polarization charge density can be broken into two terms

$$\sigma_{\text{pol}} = \rho_0 \frac{1 - \epsilon}{\epsilon} + \frac{1}{4\pi} \frac{\nabla \epsilon}{\epsilon} \cdot \nabla \phi = \sigma_{\text{pol}}^V + \sigma_{\text{pol}}^S \quad (44)$$

The first term,  $\sigma_{\text{pol}}^V = \rho_0(1 - \epsilon)/\epsilon$ , is finite everywhere  $\rho_0$  is finite and  $\epsilon \neq 1$  (the superscript “V” implies “volume”). The second term,  $\sigma_{\text{pol}}^S = (1/4\pi)\nabla \ln(\epsilon) \cdot \nabla \phi$ , is finite only in the region of the dielectric boundary (the superscript “S” implies “surface”). Under the standard assumption of most boundary element methods,  $\sigma_{\text{pol}}^V$  is taken to vanish. However, this restriction is not mandatory. The potential due to  $\rho_0$  and  $\sigma_{\text{pol}}^V$  together is the solution of the free space Poisson equation for the modified density

$$\rho_{\text{eff}} = \rho_0 + \sigma_{\text{pol}}^V = \frac{\rho_0}{\epsilon} \quad (45)$$

In the case of a charge density  $\rho_0$  contained in a cavity of constant internal dielectric  $\epsilon_1$ ,  $\rho_{\text{eff}}$  takes the form of a scaled density that can be expanded in the same basis as  $\rho_0$ . Extension to cases where the dielectric is more complicated in the region of  $\rho_0$  is possible, but for simplicity is not detailed here.

To facilitate the development, a more general scale factor than  $f(\epsilon_2)$  is introduced based on eq 21 for the polarization surface charge density,

$$f(\epsilon_1, \epsilon_2) = \frac{\epsilon_2 - \epsilon_1}{\epsilon_1 \epsilon_2} \quad (46)$$

Note that  $f(1, \epsilon_2) = f(\epsilon_2)$  defined earlier. The development is analogous to that of the previous section, with the  $\mathbf{A}$  matrix

defined as  $\mathbf{A} = \mathbf{A}_0/f(\epsilon_1, \epsilon_2)$ , and the static potential in eq 38 replaced by  $\phi_{\text{eff}} = \mathbf{B} \cdot \boldsymbol{\rho}_{\text{eff}} = (1/\epsilon_1)\phi_0$ . The equation for the surface component of the polarization density obtained from the variational procedure is

$$\sigma_{\text{pol}}^{S*} = -f(\epsilon_1, \epsilon_2) \mathbf{A}_0^{-1} \cdot \mathbf{B} \cdot \boldsymbol{\rho}_0 \quad (47)$$

and the corresponding Green's functions analogous to eqs 42 and 43, are

$$\mathbf{G}(\epsilon_1, \epsilon_2) = \left(\frac{1}{\epsilon_1}\right) \mathbf{C} - f(\epsilon_1, \epsilon_2) \mathbf{B}^T \cdot \mathbf{A}_0^{-1} \cdot \mathbf{B} \quad (48)$$

and

$$\mathbf{G}_{\text{pol}}(\epsilon_1, \epsilon_2) = \left(\frac{1 - \epsilon_1}{\epsilon_1}\right) \mathbf{C} - f(\epsilon_1, \epsilon_2) \mathbf{B}^T \cdot \mathbf{A}_0^{-1} \cdot \mathbf{B} \quad (49)$$

This model obtains the exact result in the limit  $\epsilon_1 = \epsilon_2$  and reduces to the conventional model presented earlier for  $\epsilon_1 = 1$  (eqs 42 and 43) that in principle is exact when  $\epsilon_2 = \infty$ . Moreover, the equations (if solved exactly) satisfy Gauss' law (eq 14) for any  $\epsilon_1$  and  $\epsilon_2$ .

An alternative to modeling the solute polarizability as a continuum dielectric is to employ an explicit polarizable solute model. One possibility that is currently being explored is to couple the solvation potential with the chemical potential equalization method<sup>34</sup> to model the solute polarizability.

*Use of Constraints.* The set of linear equations (eqs 38–43) uses surface element basis functions for the expansion of the polarization surface charge. Since this basis set is not complete in practice, the solution of the corresponding differential equation is approximate. Of primary concern is that the solution may not exactly satisfy constraint conditions such as Gauss' law (eq 21). More generally, the exact conductor surface charge should cancel *all* the multipole moments of the solute outside the cavity in order that the total field vanishes (see eq 33). In the case of quantum calculations where the tails of the electronic density extend outside the cavity, the integrated polarization density on the surface is not the total integrated polarization density (compare eqs 14 and 21). Consequently, it is sometimes desirable to normalize the total surface charge to be the integrated polarization charge (including the contribution outside the surface). More detailed discussions of the problem of outlying charge have been discussed elsewhere.<sup>6,28,35,36</sup> It is possible in the present approach to incorporate some of these conditions by imposing a set of linear constraints and performing a constrained variation of the surface charge density with the method of Lagrange multipliers. The general form of the equations are given in Appendix B. The result is that a constraint modification is added to the unconstrained surface charge density, and the corresponding correction to the energy can be expressed as the electrostatic self-energy of the surface charge correction, or alternately as a positive quadratic term involving the vector of Lagrange multipliers. In the limit that the surface elements become complete, the Lagrange multipliers and corresponding constraint penalty vanish.

An alternate procedure that has been suggested is to scale the approximate surface charge by the factor  $\Sigma/\tilde{\Sigma}$ , where  $\Sigma$  is the theoretical value<sup>57</sup> of the total surface charge determined by Gauss' law, and  $\tilde{\Sigma}$  is the actual computed value.<sup>17,18</sup> There are two main problems with this approach: (1) it breaks down in the limit  $\Sigma$  or  $\tilde{\Sigma}$  go to zero (since this implies scaling by zero or infinity), e.g., (for any neutral charge distribution) and

(2) analytic derivatives of the scale factor with respect to atomic positions (required for forces) and with respect to the static charge density (required in the Fock or Kohn–Sham Hamiltonian operators, see Appendix B) are not straightforward. The first problem can be avoided in the case of quantum calculations by separation of the total charge density into nuclear and electronic components. The polarization response for each density can be calculated and renormalized individually and subsequently combined to obtain the total polarization response. A drawback of this approach is that two large polarization responses are calculated that to a large extent cancel one another. This procedure could lead to numerical errors that are not size consistent when applied to very large systems, such as can now be addressed with linear-scaling electronic structure methods.

The use of explicit constraints in the variational procedure overcomes these difficulties (Appendix B). It is not clear whether inclusion of explicit physical constraints in the variational procedure (such as Gauss' law) necessarily leads to improved results for other properties such as the surface element basis becomes more complete, the variational energy is systematically lowered. Since the constrained variational procedure imposes a quadratic penalty on the total energy that vanishes in the limit that the surface element basis becomes complete, the convergence of the energy with respect to the basis is retarded by such constraints. Moreover, the potential that enters the Fock or Kohn–Sham Hamiltonian operators is *not* simply the electrostatic potential of the constrained surface charge density, but contains an additional term that is linear in the vector of Lagrange multipliers (Appendix B). A modified functional that avoids these difficulties can be constructed, but only at the cost of sacrificing the variational relationship with the polarization surface charge. This point is further discussed in section 4.

*Gradients.* An advantage of the conductor-like screening model (and other boundary element methods) over finite-difference methods for solution of the Poisson or Poisson–Boltzmann equation is that gradients for the former can be computed without recourse to mapping transformations from a three-dimensional grid.<sup>37</sup> Calculation of gradients for boundary element solvation methods in quantum mechanical applications have been discussed extensively in the literature.<sup>15,16,38–41</sup> The purpose here is to outline the general procedure and then focus on some subtleties of the surface element derivatives that make an analytic treatment difficult. In the following section a new analytic solvation method is proposed that overcomes these difficulties.

The expression for the gradient of the solvent polarization energy for “fixed” charge distributions ( $\boldsymbol{\rho}_0 \neq \boldsymbol{\rho}_0(\mathbf{R}_i)$ , e.g., (a set of atom-centered point charges that can move in space, but with magnitudes that are constant) follows from eqs 39, 40, and 43,

$$\begin{aligned} \nabla_i E_{\text{pol}} &= \left[ \frac{\partial E_{\text{pol}}}{\partial \boldsymbol{\sigma}_{\text{pol}}} \right]_{\boldsymbol{\sigma}_{\text{pol}}^*} \cdot \frac{\partial \boldsymbol{\sigma}_{\text{pol}}^*}{\partial \mathbf{R}_i} + \frac{1}{2} \boldsymbol{\sigma}_{\text{pol}}^{*T} \cdot \frac{\partial \mathbf{A}}{\partial \mathbf{R}_i} \cdot \boldsymbol{\sigma}_{\text{pol}}^* + \boldsymbol{\sigma}_{\text{pol}}^{*T} \cdot \frac{\partial \mathbf{B}}{\partial \mathbf{R}_i} \cdot \boldsymbol{\rho}_0 + \\ &\quad \left[ \frac{\partial E_{\text{pol}}}{\partial \boldsymbol{\rho}} \right]_{\boldsymbol{\rho}_0} \cdot \frac{\partial \boldsymbol{\rho}_0}{\partial \mathbf{R}_i} \\ &= \frac{1}{2} \boldsymbol{\sigma}_{\text{pol}}^{*T} \cdot \frac{\partial \mathbf{A}}{\partial \mathbf{R}_i} \cdot \boldsymbol{\sigma}_{\text{pol}}^* + \boldsymbol{\sigma}_{\text{pol}}^{*T} \cdot \frac{\partial \mathbf{B}}{\partial \mathbf{R}_i} \cdot \boldsymbol{\rho}_0 \\ &= \frac{1}{2} \boldsymbol{\rho}_0^T \cdot \frac{\partial \mathbf{G}_{\text{pol}}}{\partial \mathbf{R}_i} \cdot \boldsymbol{\rho}_0 \end{aligned} \quad (50)$$

where

$$\frac{\partial \mathbf{G}_{\text{pol}}}{\partial \mathbf{R}_i} = \mathbf{B}^T \cdot \mathbf{A}^{-1} \cdot \frac{\partial \mathbf{A}}{\partial \mathbf{R}_i} \cdot \mathbf{A}^{-1} \cdot \mathbf{B} - \left( \mathbf{B}^T \cdot \mathbf{A} \cdot \frac{\partial \mathbf{B}}{\partial \mathbf{R}_i} + \frac{\partial \mathbf{B}^T}{\partial \mathbf{R}_i} \cdot \mathbf{A} \cdot \mathbf{B} \right) \quad (51)$$

The derivative term with respect to  $\sigma_{\text{pol}}$  in eq 50 vanishes due to the variational condition of eq 37, and the derivative term with respect to  $\rho_0$  vanishes due to the fixed charge density assumption. In the more general case of a quantum mechanically derived charge density, the gradient with respect to the *total energy*  $E = E_{\text{QM}}[\rho_0] + E_{\text{pol}}[\rho_0]$ , where  $E_{\text{QM}}[\rho_0]$  is the quantum mechanical energy functional in terms of the electron density  $\rho_0$ , and  $E_{\text{pol}}[\rho_0]$  is the solvation energy functional of eq 43, can be written formally as

$$\nabla_i E = \frac{\partial E_{\text{QM}}}{\partial \mathbf{R}_i} + \frac{\partial E_{\text{pol}}}{\partial \mathbf{R}_i} + \int \left[ \frac{\partial E}{\partial \rho(\mathbf{r})} \right]_{\rho_0} \frac{\partial \rho_0(\mathbf{r})}{\partial \mathbf{R}_i} d^3 r \quad (52)$$

The first two terms make up the Hellmann–Feynman term associated with the total energy. The last term in eq 52 that involves a partial derivative with respect to the electron density that vanishes if the Hellmann–Feynman theorem is strictly obeyed. This is the case for “fixed” charge distributions (e.g., a charge vector that is independent of particle positions), empirical density-functional based methods such as chemical potential equalization,<sup>34</sup> and quantum methods that use basis functions that are independent of the atomic coordinates (i.e., do not require Pulay corrections) or in the limit that the basis set for the expansion of the wave function becomes complete. This can be illustrated by identifying the quantum mechanical chemical potential<sup>58</sup>  $\mu$  for systems constrained to a fixed number of electrons with the last energy derivative on the right-hand side of eq 52, which leads to

$$\int \left[ \frac{\partial E}{\partial \rho(\mathbf{r})} \right]_{\rho_0} \frac{\partial \rho_0(\mathbf{r})}{\partial \mathbf{R}_i} d^3 r = \mu \frac{\partial}{\partial \mathbf{R}_i} \int \rho_0(\mathbf{r}) d^3 r = 0 \quad (53)$$

Gradient corrections for non Hellmann–Feynman forces have been described extensively in the literature.<sup>42</sup> The purpose here is to present the full derivatives of the  $\mathbf{A}$  and  $\mathbf{B}$  matrixes in eq 50, and show that approximate derivative expressions that are used almost universally with conventional boundary element solvation methods contain singularities due to discontinuities in the solvation potential.

If the dependence of the surface elements on the atomic positions is neglected, the term involving the  $\mathbf{A}$  matrix in eq 50 drops out, resulting in a *fixed cavity* approximation:

$$\nabla_i E_{\text{pol}}^{(\text{FC})} = \sigma_{\text{pol}}^* \cdot \frac{\partial \mathbf{B}}{\partial \mathbf{R}_i} \cdot \rho_0 \quad (54)$$

where the partial derivative of the  $\mathbf{B}$  matrix contains only terms that involve explicitly the atomic positions (no cavity terms). Calculation of the gradient contribution due to the cavity requires an analytic expressions for the  $\mathbf{A}$  and  $\mathbf{B}$  matrix elements in terms of the atomic positions. This is often not straightforward since, for example, the diagonal  $\mathbf{A}$  matrix elements that typically depend on the area associated with individual surface elements are complicated functions of geometry in the region of atomic overlap. As regions of the surface become exposed or buried, new surface elements emerge or vanish and cause the dimensions of the  $\mathbf{A}$  and  $\mathbf{B}$  matrixes themselves to change discontinuously. A detailed discussion of the requirements for a smooth solvation potential are presented in Appendix C. The next section introduces a new method that retains the simplicity of

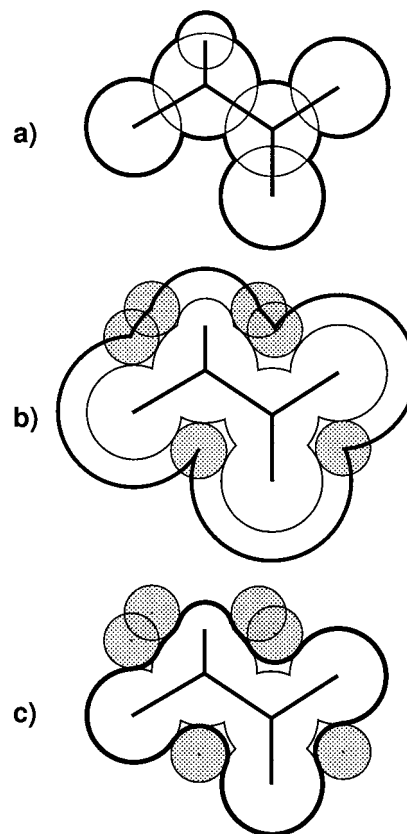


**Figure 1.** Definition of different molecular surfaces (thick lines): (a) van der Waals surface (vdWS), (b) solvent accessible surface (SAS), and (c) solvent excluded surface (SES).

the conductor-like screening model while satisfying the requirements for a smooth solvation potential.

**3.2. A Smooth Solvation Potential.** In this section, a simple analytic solvation model is proposed that overcomes many of the difficulties associated with other surface element methods. The model uses the solvent accessible surface (Figure 1) to define the boundary between the solute and solvent so that evaluation of derivatives with respect to surface element positions is simplified (Appendix C). The problem of Coulomb singularities is overcome by the use of spherical Gaussian functions of the form

$$\left( \frac{\zeta_k^2}{\pi} \right)^{3/2} e^{-\zeta_k^2 |\mathbf{r} - \mathbf{r}_k|^2} \quad (55)$$

to model surface element interactions. The electrostatic interaction between two surface element Gaussians with exponents  $\zeta_i$  and  $\zeta_j$ , respectively, centered at positions  $\mathbf{r}_i$  and  $\mathbf{r}_j$ , is given by

$$\int \int \frac{\left( \frac{\zeta_i^2}{\pi} \right)^{3/2} e^{-\zeta_i^2 |\mathbf{r} - \mathbf{r}_i|^2} \left( \frac{\zeta_j^2}{\pi} \right)^{3/2} e^{-\zeta_j^2 |\mathbf{r}' - \mathbf{r}_j|^2}}{|\mathbf{r} - \mathbf{r}'|} d^3 r d^3 r' = \frac{\text{erf}(\zeta'_{ij} r_{ij})}{r_{ij}} \quad (56)$$

where  $\zeta'_{ij} = \zeta_i \zeta_j / \sqrt{\zeta_i^2 + \zeta_j^2}$  and  $r_{ij} = |\mathbf{r}_i - \mathbf{r}_j|$ . Each atomic sphere is discretized into a set of surface elements according to the points and weights used in high-order angular quadrature schemes for spherical harmonics. This forms a natural basis for expansion of the solvent reaction-field (polarization) potential and affords significant flexibility in choosing the level of discretization. The model is calibrated by adjustment of the Gaussian exponents to obtain the exact Born solvation energy

and a uniform charge distribution for spherical ions. The matrix equations are further modified by a transformation involving a switching operation on the inverse diagonal  $\mathbf{A}$  matrix elements that allows the effect of surface elements on the energy to be smoothly switched on or off as they become exposed or buried in a manner that maintains linearity of the algebraic equations.

*Discretization of the Atomic Spheres.* The high-order angular numerical quadrature schemes with octahedral symmetry for spherical harmonic functions described by Delley<sup>43</sup> were used as a basis for discretization of the atomic spheres into surface elements. The numerical quadrature schemes provide a set of  $M$  points  $\{\hat{\mathbf{r}}_k\}$  (assumed on the unit sphere) and weights  $\{w_k\}$  that allow integrals of functions to be approximated by

$$\int_0^{2\pi} d\phi \int_0^\pi f(\hat{\mathbf{r}}) \sin(\theta) d\theta = \int f(\hat{\mathbf{r}}) d\Omega \approx \sum_k^M f(\hat{\mathbf{r}}_k) w_k \quad (57)$$

where  $\int d\Omega = \int_0^{2\pi} d\phi \int_0^\pi \sin(\theta) d\theta$ . The quadrature schemes are chosen such that the above integral is “exact” (to machine precision) if the angular function  $f(\hat{\mathbf{r}})$  can be represented by an expansion in spherical harmonic functions up to a given order  $2l_{\max} + 1$ . Hence, the numerical quadrature schemes of a given order satisfy the  $L_1$  norm conditions for  $0 \leq l \leq 2l_{\max} + 1$ ; that is,

$$\int Y_{l,m}(\hat{\mathbf{r}}) d\Omega = \sum_k^M Y_{l,m}(\hat{\mathbf{r}}_k) w_k = \sqrt{4\pi} \delta_{l,0} \quad (58)$$

and  $L_2$  orthonormality conditions for  $0 \leq l, l' \leq l_{\max}$

$$\int Y_{l,m}(\hat{\mathbf{r}}) Y_{l',m'}(\hat{\mathbf{r}}) d\Omega = \sum_k^M Y_{l,m}(\hat{\mathbf{r}}_k) Y_{l',m'}(\hat{\mathbf{r}}_k) w_k = \delta_{l,l'} \delta_{m,m'} \quad (59)$$

Spherical harmonic expansions have been used routinely for the solution of electrostatic problems since they are eigenfunctions of the angular part of the Laplacian operator in spherical polar coordinates. High-order numerical integration schemes have been extremely valuable in the solution of the Poisson equation in density-functional calculations.<sup>44,45</sup> In Gaussian-based density-functional methods, the electron density is often expanded in an auxiliary set of Gaussian functions to approximately solve for the electrostatic potential.<sup>46</sup> A variational procedure for accomplishing this involves extremizing (maximizing) the functional of eq 29.<sup>47</sup> This and related functionals have been used extensively to variationally “fit” electron densities in density-functional calculations,<sup>46</sup> determine atomic “charges” in molecules,<sup>48</sup> and numerically solve the Poisson and Poisson–Boltzmann equations.<sup>49</sup> As discussed in section 2.2, the variational procedure given by eq 29 is equivalent to the conductor variational procedure (eqs 34–37) with the restriction that the polarization density occurs only at the surface, and the electrostatic energy is minimized instead of maximized. The surface elements that are used as basis functions in the variational procedure should be chosen to give an accurate representation of the multipole expansion of the solute potential outside the cavity. For this purpose, the spherical harmonic angular quadrature schemes are particularly well suited. Angular quadrature schemes with octahedral symmetry are used with number of points/sphere ranging from 14 to 1202, corresponding to  $l_{\max} = 2$  to 29, respectively.<sup>43</sup> For each set of quadrature points  $\hat{\mathbf{r}}_k$  of a given order  $l_{\max}$  on the unit sphere, the Gaussian

**TABLE 1: Gaussian Exponents for a Unit Sphere at Different Discretization Levels<sup>a</sup>**

no. of points	$l_{\max}$	$2l_{\max} + 1$	$\zeta$	$\sigma_{\text{rms}}$
14	2	5	4.865	$8.9 \times 10^{-4}$
26	3	7	4.855	$6.9 \times 10^{-3}$
50	5	11	4.893	$3.5 \times 10^{-3}$
110	8	17	4.901	$3.8 \times 10^{-3}$
194	11	23	4.903	$2.4 \times 10^{-3}$
302	14	29	4.905	$1.9 \times 10^{-3}$
434	17	35	4.906	$1.2 \times 10^{-3}$
590	20	41	4.905	$2.7 \times 10^{-3}$
770	23	47	4.899	$5.6 \times 10^{-3}$
974	26	53	4.907	$5.9 \times 10^{-3}$
1202	29	59	4.907	$4.5 \times 10^{-4}$

<sup>a</sup> Optimized values of  $\zeta$  defined in eq 61 that give the exact Born ion energy are shown for angular quadrature schemes designated by  $l_{\max}$  defined in eqs 58 and 59. The relative deviation  $\sigma_{\text{rms}}$  is defined as  $\sigma_{\text{rms}} = \sqrt{\langle (\sigma_{\text{pol}}^* - \sigma_{\text{exact}})^2 \rangle / \langle \sigma_{\text{exact}}^2 \rangle}$  where  $\sigma_{\text{pol}}^*$  is the calculated surface charge vector,  $\sigma_{\text{exact}}$  is the “exact” surface charge vector defined as  $\sigma_{\text{exact}} = -\mathbf{w}/4\pi$ , and  $\mathbf{w}$  is the vector of angular quadrature weights for a given discretization level. Note that, as the number of points increases, the denominator  $\langle \sigma_{\text{exact}}^2 \rangle$  decreases such that the relative deviation is fairly constant. The minimum linear correlation coefficient between  $\sigma_{\text{pol}}^*$  and  $\sigma_{\text{exact}}$  is 0.99998 for the 26 point scheme.

exponents  $\zeta_k$  were chosen to obtain the exact Born solvation energy for a conductor, and to closely reproduce a “uniform” charge distribution on the surface. The latter implies that the surface element charges  $\sigma_k$  on  $\hat{\mathbf{r}}_k$  resulting from the variational procedure for a spherical ion of charge  $Q$  equal the corresponding normalized quadrature weights; i.e.,

$$\sigma_k = -Qw_k/4\pi \quad (60)$$

Initially, the Gaussian exponents that produced, to within machine precision, the Born energy and uniform charge distribution were obtained by solving a set of nonlinear equations with an iterative procedure. However, it was found that the Gaussian exponents can be well approximated by

$$\zeta_k = \zeta / \sqrt{w_k} \quad (61)$$

where  $\zeta$  is a parameter. For a given quadrature scheme, the parameter  $\zeta$  is adjusted to obtain the exact Born solvation energy, and with the above relation between the Gaussian exponents and quadrature weights (eq 61), results in a nearly uniform surface charge distribution (Table 1). Relations between the Born solvation energy and Gaussian exponents are derived in Appendix D using a simple analytic model. It is shown with the analytic model that the Gaussian exponent that gives the exact Born solvation energy varies as the square root of the number of surface elements (eq D-8). If it is assumed that the quadrature weights vary roughly inversely with the number of surface elements, it is expected that  $\zeta$  in eq 61 is roughly constant for different quadrature schemes. The values of  $\zeta$  in Table 1 range from 4.85 to 4.91, suggesting that the analytic model provides a useful qualitative description (see Appendix D for more detail). For spheres of radius  $R$ , the Gaussian exponents obey the scaling relation  $\zeta_k(R) = \zeta_k(1)/R$  that preserves the Born energy and uniform surface charge distribution. Consequently, the exponents for any radius are determined simply from the angular quadrature weights and tabulated values of  $\zeta$ .

*Construction of an Analytic Solvation Potential.* The Gaussian exponents  $\zeta_k$  and positions  $\mathbf{r}_k$  form the basis functions for the polarization surface charge, and are used to construct the matrix elements of eqs 39–43. The diagonal elements of the  $\mathbf{A}$  matrix

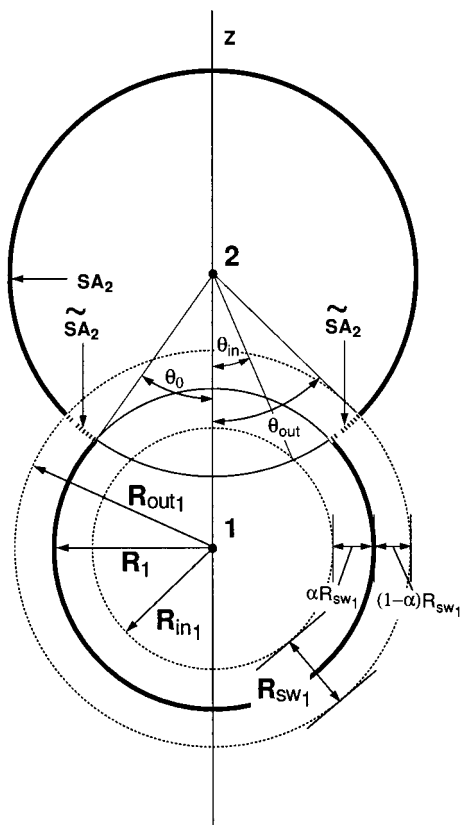


**Figure 2.** Smooth surface area model for a diatomic molecule.

represent self-energy terms of the surface elements and are analogous to the basis function “hardness” in the method of *chemical potential equalization*.<sup>34</sup> These elements impose a quadratic energy penalty associated with polarizing a particular surface element. As the diagonal **A** matrix elements go to infinity (become infinitely “hard”), no polarization occurs, and the associated basis function expansion coefficients go to zero.

This result is exploited to construct an analytic potential that allows surface elements to appear and disappear smoothly with changes in molecular geometry while maintaining the linearity of the algebraic equations. In some sense *all* of the surface element basis functions associated with each atomic sphere are considered (whether buried or on the surface), and the value of the diagonal elements of the **A** matrix are a function of the overlap with other atomic spheres. The diagonal elements are equal to the normal (calibrated) values on the solvent accessible surface and go quickly but smoothly to infinity in regions of overlap with other atomic radii as surface elements become buried. It is shown below that if the diagonal elements go to infinity, the associated off-diagonal matrix elements do not contribute to the energy and it becomes rigorous to exclude them in the algebraic equations, and thus reduce the dimensionality of the problem and greatly increase computational efficiency.

Consider a system of  $N$  atoms  $i = 1, \dots, N$ , with atomic radii  $R_i$ . The discretized solvent accessible surface is constructed by translating a unit sphere of  $M$  elements  $\hat{\mathbf{r}}_k$ ,  $k = 1, \dots, M$  to each atomic center and dilating the sphere to the radius  $R_i$ . Thus, the position of the  $k$ th surface point on atom  $i$  is  $\mathbf{r}_{ik} = \mathbf{R}_i + R_i \hat{\mathbf{r}}_k$ . A supermatrix notation is used here such that the subscript “ $ik$ ” together designates a single index for vector and matrix elements associated with the  $k$ th surface point of the  $i$ th atom; e.g., the diagonal element of the **A** matrix is denoted  $A_{ik,ik}$  (the indices  $k$  and  $l$  are used for the surface elements associated with a particular atom designated by the indices  $i$  or  $j$ ).

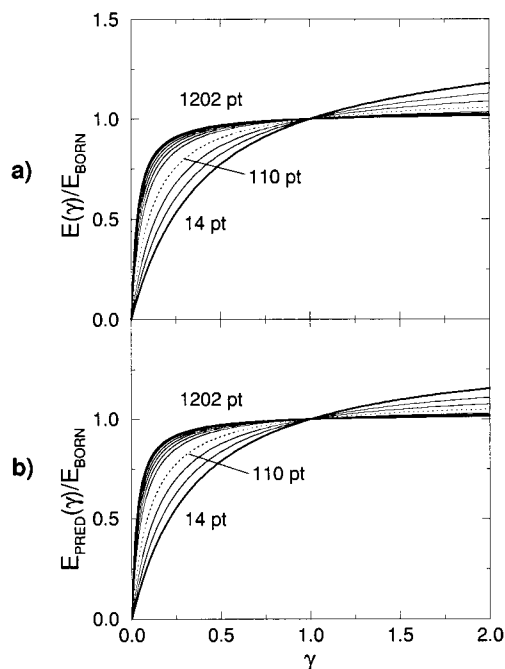


**Figure 3.** Dependence of the solvation energy on the Gaussian exponents. The figure plots the quantity  $E(\gamma)/E_{\text{BORN}}$  versus  $\gamma$  for a spherical ion at several discretization levels, where  $E(\gamma)$  is the solvation energy obtained with the set of scaled Gaussian exponents  $\zeta' = \zeta/\gamma$ , and  $\zeta$  is the calibrated value (at each discretization level) that gives the exact Born ion energy. Shown are (a) values calculated with the conductor variational procedure using the atomic surface discretization schemes given in Table 1, and (b) values predicted from the analytic model derived in Appendix A.

For a smooth representation of the solvation energy and surface charges, it is necessary to introduce basis functions (surface elements) continuously as changes in geometry bury or expose new regions of the solvent accessible surface. This is affected by scaling the basis function self-energies from their calibrated values on the surface of the cavity rapidly but smoothly to infinity as they enter the cavity. This is realized by introduction of a “switching region” (Figure 2) of thickness  $R_{\text{sw},j}$ , formed by two concentric shells on either side of the  $j$ th atomic sphere with radius  $R_j$  such that

$$R_{\text{in},j} = R_j - \alpha_j R_{\text{sw},j} \quad (62)$$

$$R_{\text{out},j} = R_j + (1 - \alpha_j) R_{\text{sw},j} \quad (63)$$

where  $\alpha_j$  is a parameter between 0 and 1. The switching function that is used is given by

$$S_{\text{wf}}(r) = \begin{cases} 0 & r < 0 \\ r^3 (10 - 15r + 6r^2) & 0 \leq r \leq 1 \\ 1 & r > 1 \end{cases} \quad (64)$$

and has the endpoint conditions

$$S_{\text{wf}}^{(1)}(0) = S_{\text{wf}}^{(1)}(1) = S_{\text{wf}}^{(2)}(0) = S_{\text{wf}}^{(2)}(1) = 0 \quad (65)$$

where  $S_{\text{wf}}^{(n)}(r) = \partial^n S_{\text{wf}} / \partial r^n$ . The off-diagonal **A**<sub>0</sub> matrix elements in the model represent electrostatic interactions between the spherical Gaussian basis functions for expansion of the polarization surface charge, and the diagonal matrix elements represent scaled (for purposes of smoothness as

discussed above) self-energies and have the form

$$(\mathbf{A}_0)_{ik,jl} = \frac{\text{erf}(\zeta'_{ik,jl}|\mathbf{r}_{ik} - \mathbf{r}_{jl}|)}{|\mathbf{r}_{ik} - \mathbf{r}_{jl}|} \quad (66)$$

$$(\mathbf{A}_0)_{ik,ik} = \frac{\zeta_{ik}}{\sqrt{2\pi}} S_{ik}^{-1} \quad (67)$$

where

$$\zeta'_{ik,jl} = \zeta_{ik}\zeta_{jl}/\sqrt{\zeta_{ik}^2 + \zeta_{jl}^2} \quad (68)$$

$$\zeta'_{ik} = \zeta/(\sqrt{w_k}R_i) \quad (69)$$

$$S_{ik} = \prod_j^{\text{atoms}} S_{\text{wf}}(\hat{r}_{ik,j}) \quad (70)$$

$$\hat{r}_{ik,j} = [|\mathbf{r}_{ik} - \mathbf{R}_j| - R_{\text{in},j}]/R_{\text{sw},j} \quad (71)$$

The  $\zeta$  parameter in eq 69 for each discretization level (quadrature scheme) are listed in Table 1. The value of  $S_{\text{wf}}(\hat{r}_{ik,j})$  in eq 70 varies between 0 and 1 and reflects the degree to which the  $ik$ th surface element (the  $k$ th surface element on the discretized atomic sphere of atom  $i$ ) has been switched off or on, respectively, by overlap with all the other atoms. The switching function  $S_{\text{wf}}(\hat{r}_{ik,j})$  is nonzero only for values of  $\hat{r}_{ik,j}$  between 0 and 1 (see eq 64), which indicates the degree to which the  $ik$ th surface element has penetrated the switching layer of atom  $j$ .

The  $\mathbf{B}$  matrix elements represent electrostatic interactions between basis functions for the solute charge density  $\rho_0$  and basis functions for the polarization surface charge density. If a point charge basis for the solute charge density is used (such as those used in conventional molecular mechanics force fields), the  $\mathbf{B}$  matrix elements have the form

$$(\mathbf{B})_{ik,j} = \frac{\text{erf}(\zeta_{ik}|\mathbf{r}_{ik} - \mathbf{R}_j|)}{|\mathbf{r}_{ik} - \mathbf{R}_j|} \quad (72)$$

The above expression for the matrix elements differ from those presented in other works that model the surface elements by point charges.<sup>15,22,26</sup> The gradients corresponding to eqs 66–72 are given by

$$\nabla_m(\mathbf{A}_0)_{ik,jl} = - \left( \frac{\text{erf}(\zeta'_{ik,jl}|\mathbf{r}_{ik} - \mathbf{r}_{jl}|)}{|\mathbf{r}_{ik} - \mathbf{r}_{jl}|} - \frac{2}{\sqrt{\pi}} \zeta'_{ik,jl} e^{-\zeta_{ik,jl}^2|\mathbf{r}_{ik} - \mathbf{r}_{jl}|^2} \right) \frac{\mathbf{r}_{ik} - \mathbf{r}_{jl}}{|\mathbf{r}_{ik} - \mathbf{r}_{jl}|^2} (\delta_{im} - \delta_{jm}) \quad (73)$$

$$\nabla_m(\mathbf{A}_0)_{ik,ik} = -(\mathbf{A}_0)_{ik,ik} \sum_j^{\text{atoms}} \frac{\partial S_{\text{wf}}(\hat{r}_{ik,j})}{\partial \hat{r}_{ik,j}} \nabla_m \hat{r}_{ik,j} \quad (74)$$

where

$$\frac{\partial S_{\text{wf}}(r)}{\partial r} = \begin{cases} 0 & r < 0 \\ 30r^2(r-1)^2 & 0 \leq r \leq 1 \\ 0 & r > 1 \end{cases} \quad (75)$$

$$\nabla_m \hat{r}_{ik,j} = \left( \frac{\mathbf{r}_{ik} - \mathbf{R}_j}{|\mathbf{r}_{ik} - \mathbf{R}_j|} \right) \frac{1}{R_{\text{sw},j}} (\delta_{im} - \delta_{jm}) \quad (76)$$

and

$$\nabla_m(\mathbf{B})_{ik,j} = - \left( \frac{\text{erf}(\zeta_{ik}|\mathbf{r}_{ik} - \mathbf{R}_j|)}{|\mathbf{r}_{ik} - \mathbf{R}_j|} - \frac{2}{\sqrt{\pi}} \zeta_{ik} e^{-\zeta_{ik}^2|\mathbf{r}_{ik} - \mathbf{R}_j|^2} \right) \frac{\mathbf{r}_{ik} - \mathbf{R}_j}{|\mathbf{r}_{ik} - \mathbf{R}_j|^2} (\delta_{im} - \delta_{jm}) \quad (77)$$

Equation 67 above involves scaling the diagonal elements of  $\mathbf{A}$  by a factor that varies between 1 and  $\infty$ , and it is not immediately evident that this allows surface element basis functions to appear smoothly with respect to the energy. The problem can be reformulated in a way that avoids the singularity at the inner shell boundary.

Consider partitioning the  $\mathbf{A}$  matrix (with scaled diagonal elements) into diagonal and off diagonal parts:

$$\mathbf{A} = (\mathbf{A}_{\text{diag}} + \mathbf{A}_{\text{off}}) = \mathbf{A}_{\text{diag}} \cdot (\mathbf{1} + \mathbf{A}_{\text{diag}}^{-1} \cdot \mathbf{A}_{\text{off}}) \quad (78)$$

and

$$\mathbf{A}^{-1} = (\mathbf{1} + \mathbf{A}_{\text{diag}}^{-1} \cdot \mathbf{A}_{\text{off}})^{-1} \cdot \mathbf{A}_{\text{diag}}^{-1} \quad (79)$$

The above expression for  $\mathbf{A}^{-1}$  does not contain singularities (unlike  $\mathbf{A}$ ) since it depends only on the inverse of the scaled diagonal elements eq 67. Since the surface charge and energy (eqs 41 and 43) rely on  $\mathbf{A}^{-1}$  and not on  $\mathbf{A}$  explicitly, these quantities can be evaluated by eq 79 without singularity problems. This expression, however, is not ideal for computation, since evaluation of  $\mathbf{A}^{-1}$  requires inversion of an unsymmetric matrix  $(\mathbf{1} + \mathbf{A}_{\text{diag}}^{-1} \cdot \mathbf{A}_{\text{off}})$ . It is advantageous to retain matrixes that are symmetric and positive definite to allow stable and efficient numerical solution of the associated linear equation via, for example, symmetric matrix inversion from a Cholesky decomposition (instead of general matrix inversion) for small matrixes, or conjugate gradient methods (instead of biconjugate methods) for direct minimization.<sup>32</sup> Thus the above equations are rewritten in the symmetric form:

$$\mathbf{A} = \mathbf{A}_{\text{diag}}^{1/2} \cdot (\mathbf{1} + \mathbf{A}_{\text{diag}}^{-1/2} \cdot \mathbf{A}_{\text{off}} \cdot \mathbf{A}_{\text{diag}}^{-1/2}) \cdot \mathbf{A}_{\text{diag}}^{1/2} \quad (80)$$

$$\mathbf{A}^{-1} = \mathbf{A}_{\text{diag}}^{-1/2} \cdot (\mathbf{1} + \mathbf{A}_{\text{diag}}^{-1/2} \cdot \mathbf{A}_{\text{off}} \cdot \mathbf{A}_{\text{diag}}^{-1/2})^{-1} \cdot \mathbf{A}_{\text{diag}}^{-1/2} \quad (81)$$

It is clear from the above equations that the effect of the transformation  $\mathbf{A}_{\text{diag}}^{-1/2} \cdot (\dots) \cdot \mathbf{A}_{\text{diag}}^{-1/2}$  is to create a null space for matrix elements corresponding to  $\mathbf{A}_{\text{diag}} = \infty$ ; i.e., this operation zeros out all rows and columns corresponding to  $(\mathbf{A}_{\text{diag}}^{-1/2})_{ik,ik} = 0$ . Consequently, the dimensionality of the problem can be reduced without approximation to that of surface element basis functions having nonzero scale factors  $S_{ik}$ . Moreover, the only appearance of the scaled diagonal elements occurs in the form of  $\mathbf{A}_{\text{diag}}^{-1/2}$  which have positive semidefinite values, and the transformed matrix  $(\mathbf{A}_{\text{diag}}^{-1/2} \cdot \mathbf{A}_{\text{off}} \cdot \mathbf{A}_{\text{diag}}^{-1/2})$  that has elements bounded by 0 and 1.

The solution for the polarization surface charge can be rewritten in the transformed reduced dimensional space as

$$\sigma_{\text{pol}}^* = -\mathbf{A}'^{-1} \cdot \mathbf{B}' \cdot \rho_0 \quad (82)$$

where

$$\begin{aligned} \mathbf{A}'^{-1} &= (\mathbf{1} + \mathbf{A}_{\text{diag}}^{-1/2} \cdot \mathbf{A}_{\text{off}} \cdot \mathbf{A}_{\text{diag}}^{-1/2})^{-1} \\ &= (\mathbf{A}_{\text{diag}}^{-1/2} \cdot \mathbf{A} \cdot \mathbf{A}_{\text{diag}}^{-1/2})^{-1} \end{aligned} \quad (83)$$

$$\mathbf{B}' = \mathbf{A}_{\text{diag}}^{-1/2} \cdot \mathbf{B} \quad (84)$$

and the (untransformed) surface charge is recovered by

$$\sigma_{\text{pol}}^* = \mathbf{A}_{\text{diag}}^{-1/2} \cdot \sigma_{\text{pol}}^* \quad (85)$$

Clearly the charge of a surface element  $ik$  is zero if  $(\mathbf{A}_{\text{diag}}^{-1/2})_{ik,ik} = 0$ .

**Switching Parameters.** The problem of discontinuities in the solvation potential as new surface elements vanish or emerge is remedied in the present model by the introduction of a switching region defined by concentric shells on either side of the van der Waals radius (Figure 2). The radii that bound the switching region,  $R_{\text{in}}$  and  $R_{\text{out}}$  defined in eqs 62 and 63, contain two parameters: the thickness of the switching region  $R_{\text{sw}}$ , and a shift parameter  $\alpha$  that determines where shells are located with respect to the van der Waals shell.

The switching layer thickness  $R_{\text{sw}_i}$  for a particular atom  $i$  is chosen to be proportional to its van der Waals radius  $R_i$ . It is further required that the proportionality constant be bounded from above by 1 to insure that  $R_{\text{sw}_i}$  does not exceed  $R_i$ . In the limit that the number of surface elements becomes infinite, the discontinuities associated with appearance of new surface elements vanish, and no switching is necessary. For a finite number of surface elements, a switching region is necessary for the potential to be smooth. The thickness of the switching region is defined to be an empirical relation

$$R_{\text{sw}_i} = \gamma_S R_i \sqrt{14/M} = \gamma R_i \quad (86)$$

where  $\gamma_S$  is the degree of switching,  $R_i$  is the atomic radius of atom  $i$ , and  $M$  is the number of points/sphere (determined by the discretization level). Equation 86 for  $R_{\text{sw}_i}$  allows the level of switching to be attenuated by adjusting the value of  $\gamma_S$  between zero (no switching) and 1 ("full" switching) such that full switching at the lowest discretization level considered ( $M = 14$ ) gives a switching radius equal to the atomic radius of that atom. The definition of  $\gamma_S$  is such that at full switching the switching radius will never exceed the radius of the atom itself.

Several empirical forms for the parameter  $\alpha$  were derived from analytic two-body models and tested. The results indicate that as long as the switching region is fairly small compared to the atomic radii, the optimal choice for  $\alpha$  is very nearly  $1/2$  (the symmetric switch is centered at the atomic radius). A slightly modified form for  $\alpha$  is proposed here that is inspired by a simple surface area model (see Appendix E). The result is

$$\alpha_i = \frac{1}{2} + \frac{R_i}{R_{\text{sw}_i}} - \sqrt{\left(\frac{R_i}{R_{\text{sw}_i}}\right)^2 - \frac{1}{28}} \quad (87)$$

where  $R_{\text{sw}_i}$  is given in eq 86. The parameter  $\alpha$  is independent of geometry and other atomic radii. The smooth model surface area can be computed as

$$SA = \sum_i^{\text{atoms}} \sum_k^M w_{ik} S_{ik} \quad (88)$$

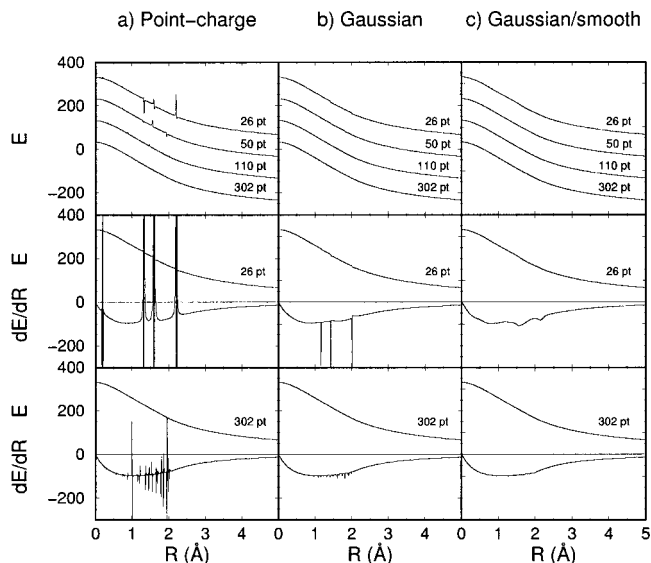


**Figure 4.** Smoothness of the solvation potential. Curves are shown at several atomic sphere discretization levels for two ions with unit radii and oppositely signed unit charges as they separate along the  $z$  axis. (a) *Point-charge* model: interactions between surface elements are modeled by point-charge interactions. (b) *Gaussian* model: interactions between surface elements are modeled by Gaussian interactions (see text). (c) *Gaussian/smooth* model: same as (b) with the addition that surface elements appear smoothly by switching on the diagonal self-interactions ( $\gamma_S = 1$ , see text). The top row shows the relative solvation energy  $E$  (kcal/mol, shifted for clarity) as a function of separation distance  $R$ , and the middle and bottom rows include the corresponding gradient curves (kcal/mol·Å) below the horizontal zero axis. Gradients were computed by finite differences ( $dE/dR = \Delta E/\Delta R$  with  $\Delta R = 0.01$  Å) to depict graphically the relative area associated with each singularity.

where  $w_{ik}$  is the  $k$ th angular quadrature weight on atom  $i$ , and  $S_{ik}$  is the switching matrix defined in eq 70.

#### 4. Numerical Tests

The following sections provide numerical tests of the proposed solvation model. In the first section, the smoothness of the potential is examined in the case of two separating ions. In the second section, the accuracy and convergence of the method are compared and the magnitude of the energy variations with regard to coordinate rotation is addressed. In the third section, results are presented for the solvation energy along the reaction coordinate of the hydrolysis of ethylene sulfate.

**4.1. Smoothness of the Potential.** The smoothness of the solvation potential with respect to changes in geometry is examined for the case of two oppositely charged ions with unit radii as they are separated along the  $z$  axis. The smoothness of the potential is affected by (1) the discretization level of the atomic spheres, (2) the occurrence of Coulomb singularities in the potential caused by overlapping surface elements modeled by point charges, and (3) discontinuities that arise from new surface elements that suddenly appear as the ions separate. Figure 4 compares the affects of each of these factors on the solvation energy curves.

For the point-charge model (Figure 4a), singularities in the potential are evident at low and medium discretization levels (26 and 50 points/sphere). Corresponding singularities in the gradient curves are more pronounced, and persist even at high discretization levels (302 points/sphere) where they correspond to jumps in energy of up to a few kcal/mol. The main source of the singularities in the gradient is the Coulomb singularity that occurs when two surface elements on different spheres are

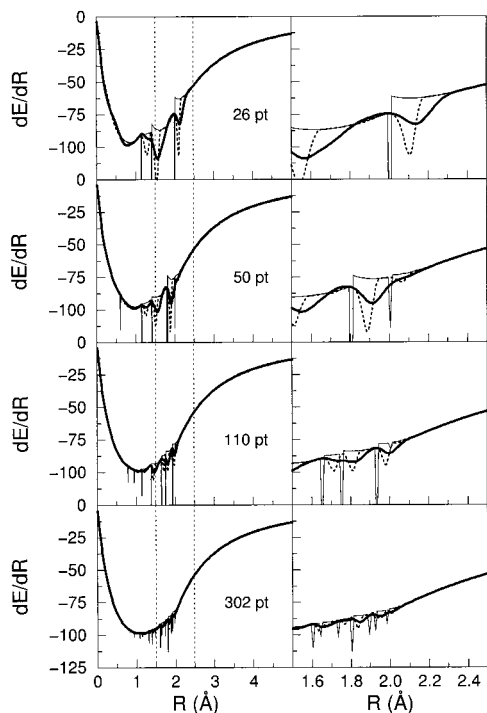


**Figure 5.** Solvation gradient curves (kcal/mol·Å) for separating ions at different discretization and smoothing levels. Discretization levels range from 26 points/atomic sphere (top) to 302 points/atomic sphere (bottom). Gradient curves are shown with no smoothing ( $\gamma_s = 0$ , thin solid line), intermediate smoothing ( $\gamma_s = 0.5$ , thin dotted line), and full smoothing ( $\gamma_s = 1$ , thick solid line). The second column shows a magnified view of the range bracketed by dotted lines in the first column.

nearly superimposed. The corresponding off-diagonal **A** matrix elements become unstable and can result in a singular matrix. These errors can make a positive or negative contribution to the gradient, and in some instances cause it to transiently change sign. This results in an artificial attractive well in the solvation energy curve that should be monotonic in the present example. Figure 4b illustrates the effect of replacing the point-charge surface element interaction model with the proposed Gaussian model. No singularities in the potential occur and the solvation energy curves are greatly improved even at low discretization levels. This is in part due to the relation between the Gaussian exponents and quadrature weights (eq 61) that result in the former being roughly proportional to the square root of the number of surface elements/atomic sphere (Appendix D); i.e., as the number of surface elements decrease, the Gaussian functions become more diffuse and result in smoother interactions at short range. However, in the absence of smoothing, singularities in the gradient that correspond to discontinuities in the solvation energy remain, especially at low discretization levels (26 points/sphere). These singularities arise from the sudden appearance of new surface elements as the ions separate. The nature of the singularity is to cause a discontinuous decrease in the solvation energy.<sup>59</sup> Figure 4c shows the effect of smoothly turning on new surface elements with the proposed method ( $\gamma_s = 1$  in eq 86). Even at low discretization levels the gradients are smooth.

Figure 5 compares the solvation energy gradients as a function of separation distance for several discretization and smoothing levels. In the case of no smoothing ( $\gamma_s = 0$ ), the gradients have singularities due to discontinuities in the potential as described above. At medium and full smoothing ( $\gamma_s = 0.5$  and 1, respectively) the gradients are smooth for all discretization

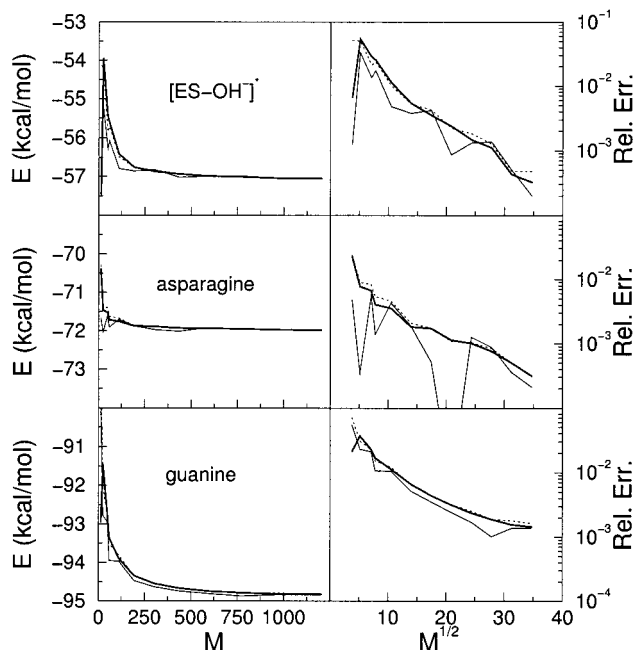


**Figure 6.** Accuracy and convergence of the solvation energy. The first column plots the solvation energy **E** (kcal/mol) as a function of **M**, the number of surface elements/atomic sphere; the second column shows the relative error (estimated relative to a discretization level of 5000 points/atomic sphere) as a function of  $M^{1/2}$  ( $M^{1/2}$  is related to the average distance between surface elements). Curves corresponding to smoothing levels  $\gamma_s = 0$  (thin solid line),  $\gamma_s = 0.5$  (thin dotted line), and  $\gamma_s = 1$  (thick solid line) are shown for the transition state intermediate in the nucleophilic attack on ethylene sulfate by a hydroxide ion  $[\text{ES-OH}]^-*$  (top), the neutral amino acid asparagine, and the negatively charged guanine 5' nucleotide phosphate.

levels. These features are important for gradient-based geometry optimizations, transition-state searches, and molecular dynamics simulations.

**4.2. Accuracy and Convergence.** In this section the accuracy and convergence of the proposed method with respect to the surface discretization level is examined, modified functionals that obey physical constraint conditions are presented, and the problem of rotational variance is discussed.

Table 2 lists the solvation energy, total surface charge, and surface area (eq 88) at smoothing levels  $\gamma_s = 0, 0.5$ , and 1 for the pentavalent transition state intermediate in the hydrolysis reaction of ethylene sulfate,  $[\text{ES-OH}]^-*$  (ref 50). At low, medium, high, and very high discretization levels (14–26, 50–110, 302–590, and 1202 points/sphere) the relative error in the solvation energy is typically less than 1%, 0.5%, 0.2%, and 0.05%, respectively. Accuracy sufficient for most chemical applications (less than 1 kcal/mol) is obtained with relatively low discretization levels; however, convergence to higher accuracy is rather slow. It is possible that further refinement of the model, such as modification of the switching scheme in eq 68, may offer improvement. Figure 6 illustrates the convergence of the solvation energy with respect to the discretization level for several molecules at various levels of switching  $\gamma_s = 0, 0.5$ , and 1. The figure supports the main conclusions derived from Table 2 with regard to the magnitude and convergence of errors. The convergence of the relative errors is more uniform with smoothing.

The exact conductor solution (i.e., in the surface element basis set limit) obeys Gauss' law (eq 21). For the discretization levels considered here, the error in the total surface charge is very small (Table 2). With no smoothing, agreement with Gauss' law is extremely good, with relative errors of approximately

**TABLE 2: Convergence of Solvation Properties with Discretization Level for [ES-OH]<sup>-</sup>\*<sup>a</sup>**

no. or points	$E_{\text{pol}}$	error	Q	error	SA	error
$\gamma_s = 0$						
14	-71.666	(-0.343)	1.003	( $2.6 \times 10^{-3}$ )	164.649	(-14.233)
26	-72.034	(0.025)	1.001	( $1.0 \times 10^{-3}$ )	159.524	(-9.108)
50	-71.609	(-0.401)	0.999	( $6.0 \times 10^{-4}$ )	154.305	(-3.889)
110	-71.699	(-0.310)	1.000	( $2.6 \times 10^{-4}$ )	149.754	(0.662)
194	-71.874	(-0.135)	1.000	( $2.0 \times 10^{-5}$ )	151.267	(-0.851)
302	-71.972	(-0.037)	1.000	( $5.0 \times 10^{-5}$ )	151.466	(-1.050)
434	-72.010	(0.001)	1.000	( $4.0 \times 10^{-5}$ )	150.914	(-0.498)
590	-71.918	(-0.091)	1.000	( $3.0 \times 10^{-5}$ )	149.951	(0.465)
770	-71.946	(-0.064)	1.000	( $1.0 \times 10^{-5}$ )	150.208	(0.208)
974	-71.983	(-0.026)	1.000	( $2.0 \times 10^{-5}$ )	150.394	(0.022)
1202	-71.994	(-0.015)	1.000	( $0.0 \times 10^{**}$ )	150.635	(-0.219)
$\gamma_s = 0.5$						
14	-70.286	(-1.723)	0.998	( $2.2 \times 10^{-3}$ )	154.305	(-3.889)
26	-71.359	(-0.650)	0.998	( $1.6 \times 10^{-3}$ )	149.411	(1.005)
50	-71.408	(-0.601)	0.998	( $1.7 \times 10^{-3}$ )	150.043	(0.373)
110	-71.675	(-0.334)	1.000	( $4.7 \times 10^{-4}$ )	149.584	(0.832)
194	-71.858	(-0.151)	1.000	( $1.2 \times 10^{-4}$ )	151.256	(-0.840)
302	-71.883	(-0.126)	1.000	( $1.5 \times 10^{-4}$ )	150.346	(0.070)
434	-71.931	(-0.078)	1.000	( $9.0 \times 10^{-5}$ )	150.514	(-0.098)
590	-71.934	(-0.075)	1.000	( $5.0 \times 10^{-5}$ )	150.261	(0.155)
770	-71.948	(-0.061)	1.000	( $3.0 \times 10^{-5}$ )	150.329	(0.087)
974	-71.973	(-0.037)	1.000	( $3.0 \times 10^{-5}$ )	150.348	(0.068)
1202	-71.987	(-0.022)	1.000	( $2.0 \times 10^{-5}$ )	150.629	(-0.213)
$\gamma_s = 1$						
14	-70.429	(-1.580)	0.992	( $8.3 \times 10^{-3}$ )	145.166	(5.250)
26	-71.617	(-0.392)	0.996	( $3.8 \times 10^{-3}$ )	145.414	(5.002)
50	-71.736	(-0.273)	0.997	( $2.9 \times 10^{-3}$ )	147.046	(3.370)
110	-71.904	(-0.105)	0.999	( $9.6 \times 10^{-4}$ )	148.621	(1.795)
194	-71.952	(-0.057)	1.000	( $3.6 \times 10^{-4}$ )	150.065	(0.351)
302	-71.943	(-0.066)	1.000	( $2.6 \times 10^{-4}$ )	149.751	(0.665)
434	-71.952	(-0.058)	1.000	( $1.6 \times 10^{-4}$ )	150.100	(0.316)
590	-71.954	(-0.055)	1.000	( $1.0 \times 10^{-4}$ )	150.133	(0.283)
770	-71.967	(-0.042)	1.000	( $8.0 \times 10^{-5}$ )	150.240	(0.176)
974	-71.978	(-0.031)	1.000	( $6.0 \times 10^{-5}$ )	150.244	(0.172)
1202	-71.989	(-0.020)	1.000	( $5.0 \times 10^{-5}$ )	150.387	(0.029)

<sup>a</sup> Solvation energy  $E_{\text{pol}}$  (kcal/mol), total surface charge  $Q$  (au), and surface area SA ( $\text{\AA}^2$ ). Corresponding errors are shown in parentheses. Errors were estimated relative to a discretization level of 5000 points/atomic sphere. Smoothing levels are indicated by  $\gamma_s$  values (see text).

**TABLE 3: Comparison of Unconstrained, Constrained, and Nonvariational Functionals<sup>a</sup>**

no. of points	$E_{\text{pol}}(0)$	error	$E_{\text{pol}}(\lambda)$	error	$E'_{\text{pol}}(\lambda)$	error
$\gamma_s = 0$						
26	-72.034	(0.025)	-72.034	(0.025)	-71.984	(0.026)
50	-71.609	(0.401)	-71.609	(0.401)	-71.639	(0.371)
110	-71.699	(0.310)	-71.699	(0.310)	-71.712	(0.297)
302	-71.972	(0.037)	-71.972	(0.037)	-71.974	(0.035)
$\gamma_s = 0.5$						
26	-71.359	(0.650)	-71.359	(0.650)	-71.438	(0.572)
50	-71.408	(0.601)	-71.408	(0.601)	-71.494	(0.515)
110	-71.675	(0.334)	-71.675	(0.334)	-71.699	(0.311)
302	-71.883	(0.126)	-71.883	(0.126)	-71.891	(0.119)
$\gamma_s = 1$						
26	-71.617	(0.392)	-71.616	(0.393)	-71.810	(0.119)
50	-71.736	(0.273)	-71.735	(0.274)	-71.882	(0.127)
110	-71.904	(0.105)	-71.904	(0.105)	-71.953	(0.057)
302	-71.943	(0.066)	-71.943	(0.066)	-71.956	(0.053)

<sup>a</sup> Solvation energy (kcal/mol) calculated from different functionals: the unconstrained functional  $E_{\text{pol}}(0)$  of eq B-3, the constrained functional  $E_{\text{pol}}(\lambda)$  of eq B-6, and the nonvariational constrained functional  $E'_{\text{pol}}(\lambda)$  of eq B-8. Corresponding errors are shown in parentheses. Errors were estimated relative to a discretization level of 5000 points/atomic sphere. Smoothing levels are indicated by  $\gamma_s$  values (see text).

0.1%, 0.05%, 0.005%, and 0.001% for low, medium, high, and very high discretization levels, respectively. For the smooth models, errors are slightly larger, especially at the low discretization levels that have larger switching regions ( $R_{\text{swj}}$  in eq 86).

One can insure that Gauss' law is obeyed by application of constraints in the energy variation with the method of Lagrange multipliers. Alternately, nonvariational functionals can be constructed that have the constraints built in (see Appendix B).

Table 3 compares the energies resulting from each of these procedures. There are almost negligible difference between the energies from the unconstrained and constrained variational functionals, the latter always bounded from above by the former. This is consistent with the previous observation that Gauss' law is very nearly satisfied in the absence of constraints. The nonvariational functional  $E'_{\text{pol}}(\lambda)$  results in energies that are comparable to the corresponding unconstrained energies in the

TABLE 4: Rotational Variance<sup>a</sup>

no. of points	$\langle E_{\text{pol}} \rangle$	$\langle \delta E_{\text{pol}} \rangle$	$E^*$	$\langle Q \rangle$	$\langle \delta Q \rangle$	$\langle \text{SA} \rangle$	$\langle \delta \text{SA} \rangle$
$\gamma_s = 0$							
26	-71.266	(0.445)	2.200	0.999	$(1.4 \times 10^{-3})$	150.775	(3.690)
50	-71.548	(0.199)	1.030	0.999	$(6.1 \times 10^{-4})$	150.207	(2.460)
110	-71.758	(0.107)	0.541	1.000	$(1.1 \times 10^{-4})$	150.454	(1.470)
302	-71.919	(0.038)	0.232	1.000	$(3.9 \times 10^{-5})$	150.547	(0.763)
$\gamma_s = 0.5$							
26	-71.134	(0.229)	1.050	0.996	$(1.2 \times 10^{-3})$	148.899	(1.970)
50	-71.471	(0.101)	0.599	0.999	$(4.8 \times 10^{-4})$	149.553	(1.230)
110	-71.699	(0.058)	0.356	1.000	$(1.2 \times 10^{-4})$	150.027	(0.862)
302	-71.887	(0.021)	0.110	1.000	$(2.4 \times 10^{-5})$	150.357	(0.424)
$\gamma_s = 1$							
26	-71.389	(0.138)	0.620	0.995	$(1.0 \times 10^{-3})$	144.813	(0.897)
50	-71.778	(0.066)	0.368	0.998	$(3.8 \times 10^{-4})$	147.210	(0.547)
110	-71.911	(0.032)	0.181	0.999	$(9.2 \times 10^{-5})$	148.872	(0.374)
302	-71.946	(0.010)	0.054	1.000	$(1.8 \times 10^{-5})$	149.881	(0.175)

<sup>a</sup> Rotational variance was computed by sampling Euler rotations in  $36^\circ$  intervals. Bracketed quantities indicate average values of the solvation energy  $E_{\text{pol}}$  (kcal/mol), total surface charge  $Q$  (au), and surface area SA ( $\text{\AA}^2$ ). Corresponding root-mean-square deviations are indicated by  $\langle \delta \dots \rangle$ . The "energy barrier"  $E^*$  (kcal/mol) is the difference between the maximum and minimum sampled energy values. Smoothing levels are indicated by  $\gamma_s$  values (see text).

case of no smoothing ( $\gamma_s = 0$ ), whereas in the case of full smoothing ( $\gamma_s = 1$ ) the functional leads to considerable improvement at low discretization levels, reducing the error by roughly a factor of 2. Further testing and comparisons are needed before one can conclude that  $E'_{\text{pol}}(\lambda)$  is a better solvation energy functional than the unconstrained variational functional.

Numerical methods that utilize surface elements or 3-dimensional grids are subject to "basis set" related errors. In particular, if the basis functions used to expand the solvation potential are not rotationally invariant, the solvation energy varies when the system is rigidly rotated. Table 4 compares the magnitude of the rotational root-mean-square deviation (rmsD) of the solvation energy, total surface charge, and surface area for  $[\text{ES-OH}^-]^*$  at several discretization levels. The rotational rmsD provides statistical information that compliments the absolute errors given in Tables 2 and 3. The rotational rmsD measures the fluctuation of a quantity for many orientations whereas the absolute error measures the error in the basis set limit for a single orientation. The rotational energy rmsD is typically lower than the absolute error of Table 2. Moreover, the rotational energy rmsD in the full smoothing model ( $\gamma_s = 1$ ) is about a factor of 2–4 smaller than in the model with no smoothing ( $\gamma_s = 0$ ). The rotational rmsD of the total surface charge at each discretization level is similar for all smoothing levels, and comparable in magnitude to the Gauss' law error in Table 2 with no smoothing. The rotational rmsD of the surface area is reduced by a factor of 2 with full smoothing relative to no smoothing, and the magnitude is significantly less than the error in Table 2. Overall, the magnitude of rotational rmsD for the solvation energy, total surface charge, and surface area are less than the corresponding basis set errors, and decrease with smoothing so that the rotational variance is not expected to be a dominant error in calculations.

**4.3. Application to Sulfate Hydrolysis.** Solvent stabilization plays an important role in reaction dynamics in solution. Quantum mechanical calculations at reliable basis set levels are currently too time-consuming to include many solvent molecules in routine transition state optimizations. Consequently, these calculations are typically performed in the gas phase and subsequently corrected to account for an approximate solvation effect.<sup>6,50</sup> Alternately, one can include the solvation potential directly in the electronic Hamiltonian and introduce solvent effects self-consistently. For an explicit solvent representation, the latter procedure is more reasonable.

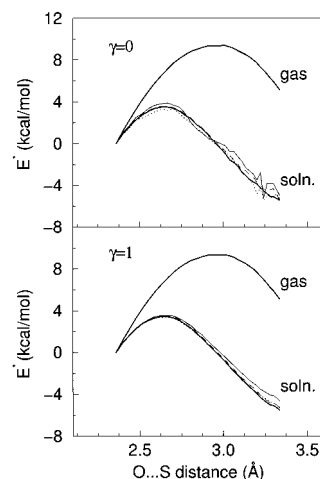


**Figure 7.** Potential energy surfaces for  $\text{OH}^-$  attack on ethylene sulfate at different levels of smoothing. Curves at several discretization levels (26, 50, 110, and 302 points/atomic sphere, corresponding to solid, dotted, dashed, and thick solid lines, respectively) are shown for smoothing levels  $\gamma_s = 0$  (no smoothing, top), and  $\gamma_s = 1$  (full smoothing, bottom).

The present solvation model is not yet integrated into a quantum mechanical electronic structure package, so that self-consistent results are not yet available. To assess the magnitude of errors in a real chemical application of the present model, the energy surface of the hydrolysis reaction of ethylene sulfate was studied. Density-functional results for the gas-phase charge density along the reaction coordinate<sup>50</sup> were used as input to calculate the solvation energy correction to the reaction profile with the present model. Figures 7 and 8 compare the gas phase and solvent corrected energy surfaces for the nucleophilic attack by  $\text{OH}^-$  on ethylene sulfate.<sup>50</sup> Only the electrostatic component of the solvation energy is considered. The overall solvation effect is to stabilize the separated reactants relative to the complex. The system has a net  $(-1)$  charge that in the reactant state resides on the hydroxide ion, and hence it is not surprising that the most solvent exposed conformations (corresponding to large separation distances) have the largest solvent stabilization. This contrasts with cases where both reactants have the same sign charge, such as a hydroxide ion attacking a negatively charged phosphate, for which the transition state is preferentially stabilized by the solvent.<sup>60</sup>

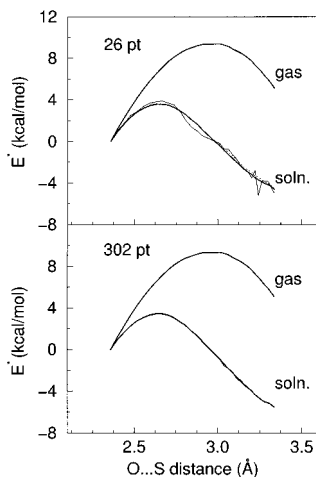


**Figure 8.** Potential energy surfaces for  $\text{OH}^-$  attack on ethylene sulfate at different atomic sphere discretization levels. Curves at several levels of smoothing ( $\gamma_s = 0, 0.5$ , and  $1$ , corresponding to solid, dotted, and thick solid lines, respectively) are shown for discretization levels of 26 points/atomic sphere (top) and 302 points/atomic sphere (bottom).

Figure 7 compares the solvation curves at different discretization levels (26, 50, 110, and 302 points/sphere) at smoothing levels  $\gamma_s = 0$  and  $1$ . With  $\gamma_s = 0$ , the curves are irregular at the lower discretization levels (26 and 50 points/sphere). With  $\gamma_s = 1$ , the curves are very smooth. The maximum difference between the curves occurs for the separated reactants where the total energies are  $-4.6$ ,  $-5.3$ ,  $-5.3$ , and  $-5.5$  kcal/mol for discretization levels of 26, 50, 110, and 302 points/sphere, respectively. Figure 8 illustrates the effect of smoothing ( $\gamma_s = 0, 0.5$ , and  $1$ ) for high and low discretization levels (26 and 302 points/sphere). At low discretization level and no smoothing, variations in the energy surface of around 2 kcal/mol occur as the  $\text{OH}^-$  and ethylene sulfate separate. At intermediate and full smoothing ( $\gamma_s = 0.5$  and  $1$ ), these variations are negligible. At high discretization level, the effect of smoothing is much less dramatic; i.e., all the curves are well behaved and almost indistinguishable. The curve corresponding to  $\gamma_s = 0$  exhibits minor variations as the reactants separate on the order of 0.1 kcal/mol. Overall, these results demonstrate that the present method improves the reaction profile in solution relative to that of a discontinuous solvation potential, especially at a low discretization level, and provide results that are within the accuracy range (0.1–1 kcal/mol) required of most chemical applications.

## 5. Conclusion

A new solvation model based on the conductor-like screening model has been introduced. The solvation energy of the model is smooth with continuous analytic derivatives; it contains no singularities and involves the solution of a set of linear equations. The model uses a solvent accessible surface for the cavity representation and smooth Gaussian basis functions to expand the reaction-field surface charge density and model Coulomb interactions between surface elements. Discretization of atomic surface elements is based on high-order angular quadrature schemes for spherical harmonics. The Gaussian exponents of the surface elements are calibrated to reproduce the exact Born energy for spherical ions and a uniform polarization surface charge density. Tests of the method demonstrate that it is accurate in describing the dielectric response of a conductor, and with a simple correction can be

extended to model finite dielectric materials such as liquid water with reasonable accuracy. Extensions of the method to incorporate variational constraints and to model smooth surface areas have been presented, as well as the generalization to arbitrary internal dielectric constants. It is anticipated that once integrated with quantum mechanical or molecular mechanical programs, the model will be an effective tool for the description of molecules in solution.

**Acknowledgment.** The authors acknowledge Prof. Bernard Delley for providing code for the angular quadrature schemes, Dr. Xavier Lopez for providing data on the ethylene sulfate hydrolysis reaction, and Dr. Michael Schaefer for useful discussions. Postdoctoral support for DY was provided by the National Institutes of Health (Harvard) and EMBO (ULP, Strasbourg). The laboratory is supported in part by the CNRS ESA 7006, by the Ministère de l'Éducation Nationale, by a grant from the Association pour la Recherche contre le Cancer (France). The work was also funded in part by a grant from the National Science Foundation (MK).

## Appendix A

### Polarization Charge Density at a Dielectric Discontinuity.

In this appendix the limiting behavior of a surface charge density arising from a dielectric discontinuity under the boundary conditions of eqs 16 and 17 is addressed; i.e., the connection between eqs 13 and 20 is formed in this limit. The definition of the electric displacement in a linear isotropic (dipole) polarizable medium is

$$\mathbf{D} = \mathbf{E} + 4\pi\mathbf{P} = \epsilon\mathbf{E} \quad (\text{A-1})$$

The polarization  $\mathbf{P}$  can be expressed in terms of the dielectric function and electric displacement as

$$\mathbf{P} = \frac{\mathbf{D} - \mathbf{E}}{4\pi} = \left(\frac{\epsilon - 1}{4\pi}\right)\mathbf{E} = \left(\frac{\epsilon - 1}{4\pi\epsilon}\right)\mathbf{D} \quad (\text{A-2})$$

from which the polarization charge density becomes

$$\sigma_{\text{pol}} = -\nabla \cdot \mathbf{P} = -\nabla \cdot \left(\frac{\epsilon - 1}{4\pi\epsilon}\right) \cdot \mathbf{D} - \left(\frac{\epsilon - 1}{\epsilon}\right)\rho_0 \quad (\text{A-3})$$

This equation is equivalent to eq 13 derived previously. Consider the case of a dielectric function that varies rapidly but continuously from  $\epsilon_1$  in region 1 to  $\epsilon_2$  in region 2 across a boundary layer of thickness  $\Delta x = x_2 - x_1$  in the direction  $\mathbf{n}_{21}$  normal to the layer. If the variation in the dielectric across the boundary is linear, then

$$\epsilon(x) = \epsilon_1 \frac{x_2 - x}{\Delta x} + \epsilon_2 \frac{x - x_1}{\Delta x} \quad (\text{A-4})$$

with corresponding gradient

$$\nabla\epsilon(x) = \frac{\epsilon_2 - \epsilon_1}{\Delta x} \mathbf{n}_{21} \quad (\text{A-5})$$

Using eqs A-4 and A-5, the terms involving  $\epsilon$  in eq A-3 are given by

$$-\nabla \left( \frac{\epsilon - 1}{4\pi\epsilon} \right) = -\frac{1}{4\pi} \frac{\nabla\epsilon}{\epsilon^2} = -\frac{1}{4\pi} \frac{(\epsilon_2 - \epsilon_1)\Delta x}{(\epsilon_2(x - x_1) + \epsilon_1(x_2 - x))^2} \mathbf{n}_{21} \quad (\text{A-6})$$

$$-\left( \frac{\epsilon - 1}{\epsilon} \right) = \frac{\epsilon_2(x - x_1) + \epsilon_1(x_2 - x) - \Delta x}{\epsilon_1(x_2 - x) + \epsilon_2(x - x_1)} \quad (\text{A-7})$$

The integrated polarization charge through the boundary layer (along the normal direction  $\mathbf{n}_{21}$ ) is

$$\int_{x_1}^{x_2} \sigma_{\text{pol}}(x) dx = -\frac{1}{4\pi} \int_{x_1}^{x_2} \frac{\nabla\epsilon}{\epsilon^2} \cdot \mathbf{D} dx - \int_{x_1}^{x_2} \left( \frac{\epsilon - 1}{\epsilon} \right) \rho_0 dx \quad (\text{A-8})$$

If the static charge density  $\rho_0$  contains no explicit surface charge density  $\sigma_0$  at the dielectric boundary, i.e., it is smooth in this region, then the normal component of the electric displacement is also smooth since it satisfies the Maxwell relation eq 9. In the limit the boundary layer thickness goes to zero, both  $\mathbf{D} \cdot \mathbf{n}_{21}$  and  $\rho_0$  are constant and can be taken out of the integral, leading to

$$\begin{aligned} \lim_{\Delta x \rightarrow 0} \int_{x_1}^{x_2} \sigma_{\text{pol}}(x) dx &= -\frac{1}{4\pi} \left( \int_{x_1}^{x_2} \frac{(\epsilon_2 - \epsilon_1)\Delta x}{(\epsilon_2(x - x_1) + \epsilon_1(x_2 - x))^2} dx \right) \mathbf{D} \cdot \mathbf{n}_{21} \\ &+ \left( \int_{x_1}^{x_2} \frac{\epsilon_2(x - x_1) + \epsilon_1(x_2 - x) - \Delta x}{\epsilon_1(x_2 - x) + \epsilon_2(x - x_1)} dx \right) \rho_0 \\ &= -\frac{1}{4\pi} \left( \frac{1}{\epsilon_1} - \frac{1}{\epsilon_2} \right) \mathbf{D} \cdot \mathbf{n}_{21} + \Delta x \left( 1 + \frac{\log(\epsilon_1/\epsilon_2)}{\epsilon_2 - \epsilon_1} \right) \rho_0 \\ &= -\frac{1}{4\pi} \left( \frac{\epsilon_2 - \epsilon_1}{\epsilon_1\epsilon_2} \right) \mathbf{D} \cdot \mathbf{n}_{21} = \sigma_{\text{pol}} \quad (\text{A-9}) \end{aligned}$$

which is identical to the expression of eq 20.

## Appendix B

**Constrained Variations.** Consider the set of  $N_c$  constraint conditions on the surface charge of the form

$$\mathbf{D}^T \cdot \boldsymbol{\sigma}_{\text{pol}} = \mathbf{Z} \cdot \boldsymbol{\rho}_0 = \mathbf{y} \quad (\text{B-1})$$

where  $\boldsymbol{\sigma}_{\text{pol}}$  and  $\boldsymbol{\rho}_0$  are  $M \times 1$  and  $N \times 1$  vectors representing the polarization surface charge and static charge densities (see section 3.1), respectively,  $\mathbf{D}$ ,  $\mathbf{Z}$ , and  $\mathbf{y}$  have dimensions  $M \times N_c$ ,  $N_c \times N$ , and  $N_c \times 1$ , respectively, and define the  $N_c$  constraint conditions such that the  $i$ th constraint is given by  $\sum_j D_{ji} \sigma_{\text{pol}j} = y_i$ . It is assumed that the constraint values are linear functions of the static density; i.e.,  $\mathbf{y} = \mathbf{Z} \cdot \boldsymbol{\rho}_0$ . For example, the Gauss' law constraint on the total surface charge, assuming the surface and static charge densities are expanded in a basis of  $L_1$  normalized functions, corresponds to  $N_c = 1$ ,  $D_{i,1} = 1$ , and

$Z_{1,i} = -1$  (which implies  $y_1 = -Q_0$ ). The constrained variational condition is

$$\delta \{ E_{\text{pol}}(0) - \boldsymbol{\lambda}^T \cdot (\mathbf{D}^T \cdot \boldsymbol{\sigma}_{\text{pol}} - \mathbf{y}) \} = 0 \quad (\text{B-2})$$

where

$$E_{\text{pol}}(0) = \frac{1}{2} \boldsymbol{\sigma}_{\text{pol}}^T \cdot \mathbf{A} \cdot \boldsymbol{\sigma}_{\text{pol}} + \boldsymbol{\sigma}_{\text{pol}}^T \cdot \mathbf{B} \cdot \boldsymbol{\rho}_0 \quad (\text{B-3})$$

with solution

$$\boldsymbol{\sigma}_{\text{pol}}^*(\boldsymbol{\lambda}) = -\mathbf{A}^{-1} \cdot (\mathbf{B} \cdot \boldsymbol{\rho}_0 - \mathbf{D} \cdot \boldsymbol{\lambda}) = \boldsymbol{\sigma}_{\text{pol}}^*(0) + \boldsymbol{\delta} \boldsymbol{\sigma}_{\text{pol}}^*(\boldsymbol{\lambda}) \quad (\text{B-4})$$

and

$$\begin{aligned} \boldsymbol{\lambda} &= (\mathbf{D}^T \cdot \mathbf{A}^{-1} \cdot \mathbf{D})^{-1} \cdot (\mathbf{Z} + \mathbf{D}^T \cdot \mathbf{A}^{-1} \cdot \mathbf{B}) \cdot \boldsymbol{\rho}_0 \\ &= \mathbf{Q}^{-1} \cdot \mathbf{R} \cdot \boldsymbol{\rho}_0 \quad (\text{B-5}) \end{aligned}$$

where the matrixes  $\mathbf{Q} = \mathbf{D}^T \cdot \mathbf{A}^{-1} \cdot \mathbf{D}$  and  $\mathbf{R} = (\mathbf{Z} + \mathbf{D}^T \cdot \mathbf{A}^{-1} \cdot \mathbf{B})$  have been introduced,  $\boldsymbol{\sigma}^*(0) = -\mathbf{A}^{-1} \cdot \mathbf{B} \cdot \boldsymbol{\rho}_0$  is the unconstrained surface charge vector, and  $\boldsymbol{\delta} \boldsymbol{\sigma}_{\text{pol}}^*(\boldsymbol{\lambda}) = \mathbf{A}^{-1} \cdot \mathbf{D} \cdot \boldsymbol{\lambda}$  is the constraint correction. Substituting this expression into the energy equation leads to

$$\begin{aligned} E_{\text{pol}}(\boldsymbol{\lambda}) &= \frac{1}{2} \boldsymbol{\sigma}_{\text{pol}}^*(0)^T \cdot \mathbf{B} \cdot \boldsymbol{\rho}_0 + \frac{1}{2} \boldsymbol{\delta} \boldsymbol{\sigma}_{\text{pol}}^*(\boldsymbol{\lambda})^T \cdot \mathbf{A} \cdot \boldsymbol{\delta} \boldsymbol{\sigma}_{\text{pol}}^*(\boldsymbol{\lambda}) \\ &= E_{\text{pol}}(0) + \frac{1}{2} \boldsymbol{\lambda}^T \cdot \mathbf{Q} \cdot \boldsymbol{\lambda} \\ &= \frac{1}{2} \boldsymbol{\rho}_0^T \cdot [\mathbf{G}_{\text{pol}}(0) + \boldsymbol{\delta} \mathbf{G}_{\text{pol}}(\boldsymbol{\lambda})] \cdot \boldsymbol{\rho}_0 = \frac{1}{2} \boldsymbol{\rho}_0^T \cdot \mathbf{G}_{\text{pol}}(\boldsymbol{\lambda}) \cdot \boldsymbol{\rho}_0 \quad (\text{B-6}) \end{aligned}$$

where  $\mathbf{G}_{\text{pol}}(\boldsymbol{\lambda}) = \mathbf{G}_{\text{pol}}(0) + \boldsymbol{\delta} \mathbf{G}_{\text{pol}}(\boldsymbol{\lambda})$  is the Green's function of the constrained variational procedure,  $\mathbf{G}_{\text{pol}}(0) = -\mathbf{B}^T \cdot \mathbf{A}^{-1} \cdot \mathbf{B}$  is the unconstrained Green's function (underscored by the zero argument) of eq 43, and  $\boldsymbol{\delta} \mathbf{G}_{\text{pol}}(\boldsymbol{\lambda}) = \mathbf{R}^T \cdot \mathbf{Q}^{-1} \cdot \mathbf{R}$  is the constraint correction. It is clear from the above equation that the energy of the constrained solution is equal to the unconstrained solution (eq 43) plus a positive quadratic term involving the vector of Lagrange multipliers  $\boldsymbol{\lambda}$ . This term is equal to the electrostatic self-energy of the constraint surface charge correction  $\boldsymbol{\delta} \boldsymbol{\sigma}_{\text{pol}}^*(\boldsymbol{\lambda})$ . In the limit that the surface elements become complete, the Lagrange multipliers and corresponding constraint penalty vanish.

It is noteworthy to discuss some implications of using the constrained variational functional of eq B-6. It might be argued that this functional is favorable since it results in a surface charge vector that rigorously satisfies the constraint conditions (such as Gauss' law, for example), and consequently the reaction field that is produced may be more realistic in terms of affecting a polarization response in the solute. However, this is *not necessarily* the case. In quantum mechanical calculations where the polarization of the solute is itself determined from a variational principle, the reaction field potential that enters the

Fock or Kohn–Sham Hamiltonian operators is defined (in the basis of  $\rho_0$ ) by

$$\begin{aligned} \mathbf{v}_{\text{RF}} &= \frac{\delta E_{\text{pol}}(\lambda)}{\delta \rho_0} \\ &= \mathbf{G}_{\text{pol}}(\lambda) \cdot \rho_0 \\ &= \mathbf{B}^T \cdot \boldsymbol{\sigma}_{\text{pol}}^*(0) + (\mathbf{B}^T + \mathbf{Z}^T \cdot \mathbf{Q}^{-1} \cdot \mathbf{D}^T) \cdot \delta \boldsymbol{\sigma}_{\text{pol}}^*(\lambda) \\ &= \mathbf{B}^T \cdot \boldsymbol{\sigma}_{\text{pol}}^*(\lambda) + \mathbf{Z}^T \cdot \boldsymbol{\lambda} \end{aligned} \quad (\text{B-7})$$

In the above equation, the quantities  $\mathbf{B}^T \cdot \boldsymbol{\sigma}_{\text{pol}}$  represent the electrostatic potential of the surface charge density  $\boldsymbol{\sigma}_{\text{pol}}$ . The reaction field potential of the constrained variational energy functional is equal to the electrostatic potential of the resulting surface charge density  $\boldsymbol{\sigma}_{\text{pol}}^*(\lambda)$  plus the constraint term  $\mathbf{Z}^T \cdot \boldsymbol{\lambda}$ . Consequently, the potential that enters the Fock or Kohn–Sham Hamiltonian operators is the electrostatic potential of the surface charge *only in the absence of constraints*; i.e.,  $\boldsymbol{\lambda} = 0$ .

Alternately, one can consider the modified energy functional

$$\begin{aligned} E'_{\text{pol}}(\lambda) &= \frac{1}{2} \rho_0^T \cdot \mathbf{B}^T \cdot \boldsymbol{\sigma}_{\text{pol}}^*(\lambda) \\ &= -\frac{1}{2} \rho_0^T \cdot \mathbf{B}^T \cdot \mathbf{A}^{-1} \cdot \mathbf{B}' \cdot \rho_0 \\ &= \frac{1}{2} \rho_0^T \cdot \mathbf{G}'_{\text{pol}}(\lambda) \cdot \rho_0 \end{aligned} \quad (\text{B-8})$$

where  $\mathbf{G}'_{\text{pol}}(\lambda) = -\mathbf{B}^T \cdot \mathbf{A}^{-1} \cdot \mathbf{B}'$  and  $\mathbf{B}' = \mathbf{B} - \mathbf{D} \cdot \mathbf{Q}^{-1} \cdot \mathbf{R}$ . This functional produces the reaction field potential

$$\mathbf{v}_{\text{RF}} = \frac{\delta E'_{\text{pol}}}{\delta \rho_0} = \mathbf{G}'_{\text{pol}}(\lambda) \cdot \rho_0 = \mathbf{B}^T \cdot \boldsymbol{\sigma}_{\text{pol}}^*(\lambda) \quad (\text{B-9})$$

that is the electrostatic potential of the constrained polarization surface charge vector  $\boldsymbol{\sigma}_{\text{pol}}^*(\lambda)$ . Unlike the functional  $E_{\text{pol}}(\lambda)$  of eq B-6, the modified energy  $E'_{\text{pol}}(\lambda)$  is not related by a variational principle to the surface charge vector  $\boldsymbol{\sigma}_{\text{pol}}^*(\lambda)$ . At low surface discretization levels, it is observed that the functional  $E'_{\text{pol}}(\lambda)$  often provides energies closer to the “exact” energy in the basis set limit than either  $E_{\text{pol}}(0)$  or  $E_{\text{pol}}(\lambda)$ .

## Appendix C

**Continuous Gradients for Solvation Potentials.** The purpose of this appendix is to discuss the requirements for a boundary element solvation potential to be smooth; i.e., have continuous, nonsingular derivatives with respect to the atomic positions. These conditions are essential for the stability of numerical procedures such as geometry optimizations, transition state searches, and molecular dynamics calculations. Almost universally, conventional boundary element methods do not satisfy these requirements.

The derivatives with respect to the  $\mathbf{A}$  and  $\mathbf{B}$  matrixes of eqs 39–43 depend on the definition of the surface that defines the dielectric boundary. Three types of surfaces are most commonly employed (Figure 1). The *van der Waals surface* is the closed surface that encapsulates the volume created by overlapping atom-centered van der Waals spheres. The *solvent accessible surface* is the surface created by the center of a solvent probe that makes contact everywhere on the outside of the van der Waals surface. For water, the radius is typically taken to be 1.4

Å. The van der Waals and solvent accessible surfaces are mathematically identical in their construction.<sup>61</sup> The solvent excluded surface is generated by the contact of the surface of the solvent probe with the van der Waals surface.

The van der Waals and solvent accessible surfaces have the advantage that evaluation of many of the derivative terms is straightforward since the position of each surface element is related to a unique atom position by a fixed translation (although the surface element area and its associated derivatives are more complicated, as discussed below). A disadvantage of these surfaces is that surface elements centered on adjacent atoms can overlap, and Coulomb interactions modeled by point charge interactions between surface elements can diverge. A suggested method to counter this problem is to excise surface elements in the grooves formed by overlapping spheres that results in separated patches of atomic surface area.<sup>15</sup> The solvent excluded surface, on the other hand, is smooth and avoids many of the problems of overlapping surface elements; however, the mapping between elements and atomic positions is significantly more complicated, and the derivatives are correspondingly more involved.<sup>14</sup>

An analytic mapping between surface element positions and atomic positions is a necessary but not sufficient condition to ensure that the solvation potential is smooth and has continuous, nonsingular derivatives. Conformational changes can cause new regions of the molecule to become exposed to solvent or buried, and consequently new surface elements to appear or disappear in the equations for the solvation energy.<sup>62</sup> Consequently, an additional requirement for a smooth solvation potential is that new surface elements enter or exit the expansion of the polarization surface charge density smoothly with respect to the energy. As will be shown in the next section (eq 81), a sufficient condition to satisfy the smoothness criteria is that the magnitude of the inverse diagonal  $\mathbf{A}$  matrix elements (or the analogous matrix elements in other boundary element methods) vanish smoothly when a new surface element enters the expansion of the polarization surface charge density. This behavior *can* be accommodated by a model in which the diagonal matrix elements vary inversely with the area of the corresponding surface element. There are two practical difficulties with this strategy: (1) *The calculation of surface element areas and their derivatives is complicated and computationally expensive.* An exact analytic representation of *atomic surface areas* using the Gauss–Bonnet theorem for a solvent accessible surface is considerably costly, and has prompted the development of more efficient approximate methods.<sup>51</sup> The case of calculation of the area of *individual surface elements* (modeled by curved polyhedra) is more difficult than for atomic surface areas, and extension to solvent excluded surfaces is more difficult still. Considerable effort and progress has been made to derive expressions for surface element areas and their derivatives for certain types of surface elements (sometimes referred to as *tesserae*)<sup>14</sup> for use in boundary element solvation methods.<sup>18</sup> These expressions were derived for a *given set of tesserae* generated from a numerical *tessellation procedure* for partitioning the molecular surface into surface elements. (2) *The tessellation procedure used to determine the surface elements must be smooth.* In order for the solvation potential to be a smooth analytic function, the *tessellation* procedure must proceed in a manner such that the area of each tessera can vanish and appear smoothly. The optimal partition scheme in terms of efficiency<sup>52</sup> is not necessarily smooth, since this would force many tesserae to have relatively small area. In light of these difficulties, a frequently employed approximation is to neglect

entirely the derivative contribution from the surface element areas (e.g., the diagonal  $\mathbf{A}$  matrix elements).<sup>16</sup> Although the conductor-like screening model has been used in the present discussion to outline difficulties associated with constructing an analytic boundary element solvation potential, the problem is directly analogous and equally relevant in other boundary element methods such as the polarizable continuum model.<sup>16</sup> In the following section, a relatively simple scheme that overcomes these difficulties is presented. The remainder of this section provides a brief description of gradient calculations with other (non boundary-element) solvation methods.

The problem of defining surface element derivatives does not arise in methods based on the generalized Born equation,<sup>3,7,12,53</sup> finite difference or finite element solution of the Poisson–Boltzmann equation, or in higher level integral equation theories.<sup>4,5</sup> Hence, the definition and calculation of a smooth solvation potential is less problematic for these methods. The solvation potential in methods based on the generalized Born equation has the form of an effective analytic pairwise potential. These models are practical and effective for many applications,<sup>7</sup> but it is not yet clear how they perform in applications to very large molecules. For grid-based solutions of the Poisson–Boltzmann equation, the “surface” at the dielectric discontinuity in boundary element methods is replaced by a smooth dielectric function defined, for example, as

$$\epsilon(\mathbf{r}) = \epsilon_1 + (\epsilon_2 - \epsilon_1) \exp\left[-\sum_i \beta u_i(\mathbf{r} - \mathbf{R}_i)\right] = \epsilon_1 + (\epsilon_2 - \epsilon_1) H(\mathbf{r}; \{\mathbf{R}_i\}) \quad (\text{C-1})$$

where  $\beta = 1/k_B T$ ,  $k_B$  is the Boltzmann constant,  $T$  is the temperature, and the  $u_i(r)$  are atomic energy-like functions that define the volume exclusion function  $H(\mathbf{r}; \{\mathbf{R}_i\})$ .<sup>37</sup> The smoothness of the dielectric implies the polarization density occupies a volume in regions of changing dielectric (eq 13). The Poisson–Boltzmann equation is a highly approximate and computationally efficient example of a more general class of *integral equation* methods.<sup>5</sup> Methods based on integral equation theory of solutions take into account the exclusion of solvent from the solute volume with an exponential term in the solvent probability distribution function,

$$P(\mathbf{r}) \sim e^{-\beta W(\mathbf{r})} \quad (\text{C-2})$$

where  $W(\mathbf{r})$  is the potential of mean force. In the region where solute and solvent particles overlap,  $W(\mathbf{r})$  goes to infinity, and the solvent probability goes to zero. These higher level theories are powerful techniques for describing solvation properties; however, the solution of the integral equations is much more difficult and expensive to compute for large systems in three dimensions than are boundary element methods. A strategy similar to that of eq C-2 could be adopted in a boundary element framework; however, it is desirable to maintain the advantage of the linearity of the equations and the use of simple Coulomb interactions for which efficient linear-scaling methods exist.

Simple continuum solvation models can in principle offer an alternate strategy to the application of more expensive integral equation theories or explicit simulation of the full solvent environment. The former methods are very useful in the regime where the electrostatic effects of the external environment are well approximated by a dielectric continuum. A recent paper has suggested that estimations of the free energy of solvation derived from *any* of several continuum models are comparable for a given parametric fit; the most important factor relating to whether the molecule forms a hydrogen bond or not.<sup>54</sup> A strategy

in the case of large biomolecules where structural water plays an important role is to treat explicitly the ordered solvent layers, and model the region outside by a dielectric continuum.<sup>55</sup> The construction of hybrid potentials that model different parts of a large system with different levels of theory has been successful in many areas of computational chemistry.

## Appendix D

**Dependence of Born Energy on Gaussian Exponents.** In this appendix a model is derived that provides analytic equations for the relationship between the Gaussian exponents  $\zeta_k$ , the number of discretized surface points  $M$ , and the scaled Born energy  $E_{\text{Born}}(\gamma) = (\gamma/2)Q^2/R$ .

In the present method, the solvation of a spherical ion of charge  $Q$  and radius  $R$  is modeled by a set of  $M$  spherical Gaussian functions at discretized points on the surface. These Gaussian functions serve as basis functions for the induced reaction-field surface charge, which is determined as a solution to the variational condition for the energy (eq 37). The matrix solution (eq 41) requires computation of the inverse of the  $\mathbf{A}$  matrix that contains the Gaussian–Gaussian Coulomb interactions between surface elements and hence depends on the number of Gaussian functions and their placement on the surface, as well as on their exponents. It is not difficult to solve numerically for the Gaussian exponents that give the exact Born solvation energy and uniform charge density; however, for the purposes of discussion, it is instructive to derive analytic equations for a simple model that captures the essential features of the applied method.

Consider a spherical model of  $M$  surface elements. For a unit sphere with a charge  $Q$  at its center, a representative surface element is modeled by the surface arc that is excised by a cutting plane perpendicular to the  $z$  axis corresponding to the polar angle  $0 \leq \theta \leq \theta_0$ . If the remainder of the sphere has a uniform surface charge density  $\sigma_{\text{pol}}/4\pi$ , the potential at the center of the surface element ( $\theta = 0$ ) due to the surface charge is given by

$$\phi_0(\sigma_{\text{pol}}, \theta_0) = \int_0^{2\pi} \int_{\theta_0}^{\pi} \frac{\sigma_{\text{pol}}/4\pi}{2 \sin(\theta/2)} \sin(\theta) \, d\theta \, d\phi = \sigma_{\text{pol}} - \sigma_{\text{pol}} \sin(\theta_0/2) \quad (\text{D-1})$$

and the surface area is

$$\text{Area}(\theta_0) = \int_0^{2\pi} \int_0^{\theta_0} \sin(\theta) \, d\theta \, d\phi = 2\pi[1 - \cos(\theta_0)] = 4\pi \sin^2(\theta_0/2) \quad (\text{D-2})$$

If the sphere is discretized into  $M$  surface elements, the area of each element is  $4\pi/M$ . Substitution into the above equation for the surface area gives  $\theta_0$  for a given number of surface elements  $M$  per sphere:

$$\theta_0(M) = 2\sin^{-1}(1/\sqrt{M}) \quad (\text{D-3})$$

and the expression for  $\phi_0$  above can be written in terms of  $M$  as

$$\phi_0(\sigma_{\text{pol}}, M) = \sigma_{\text{pol}} - \sigma_{\text{pol}}/\sqrt{M} \quad (\text{D-4})$$

The self-energy of each surface element is taken to be the Coulomb self-energy of a Gaussian charge density with

exponent  $\zeta$ ; i.e.,  $E_{\text{self}} = (1/2)\zeta\sqrt{2/\pi}$ . This allows energy expression to be written as

$$E(\sigma_{\text{pol}}) = \frac{1}{2}\sigma_{\text{pol}}^2\zeta\sqrt{2/\pi} + \sigma_{\text{pol}}\phi_0 + Q\sigma_{\text{pol}} = \frac{1}{2}\sigma_{\text{pol}}^2\left(\frac{M - \sqrt{M} + \zeta\sqrt{2/\pi}}{M}\right) + Q\sigma_{\text{pol}} \quad (\text{D-5})$$

Solution of the variational condition  $\delta E/\delta\sigma_{\text{pol}} = 0$  leads to

$$\sigma_{\text{pol}}^* = -Q\left(\frac{M}{M - \sqrt{M} + \zeta\sqrt{2/\pi}}\right) \quad (\text{D-6})$$

and energy

$$E(\sigma_{\text{pol}}^*) = -\frac{1}{2}Q^2\left(\frac{M}{M - \sqrt{M} + \zeta\sqrt{2/\pi}}\right) \quad (\text{D-7})$$

The value of  $\sigma_{\text{pol}}^*$ , and hence the energy  $E(\sigma_{\text{pol}}^*)$ , depends on the number of surface points  $M$  and Gaussian exponent  $\zeta$ . For a given value of  $M$ , the total energy is required to be equal to the Born solvation energy for a conductor  $E(\sigma_{\text{pol}}^*(\zeta)) = -Q^2/2$ . The solution is

$$\zeta = \sqrt{\frac{M\pi}{2}} \quad (\text{D-8})$$

With this choice of  $\zeta$ , the surface charge  $\sigma_{\text{pol}}^*(\zeta) = -Q$  is in accord with Gauss' law (eq 21). The above equations establish relationships between the total energy  $E$ , the Gaussian exponents  $\zeta$ , and the number of surface elements  $M$ . In particular, it allows us to assess how sensitive  $E$  is with respect to variations in  $\zeta$  for a given value of  $M$ . This can be quantified by looking at the ratio of the scaled energy  $E(\gamma) = E(\sigma_{\text{pol}}^*(\zeta/\gamma))$  resulting from division of  $\zeta$  by a factor  $\gamma$  with the corresponding unscaled value  $E(1) = E_{\text{Born}}$ ,

$$E(\zeta/\gamma)/E_{\text{Born}} = \frac{\gamma}{\frac{1}{\sqrt{M}} + \left(1 - \frac{1}{\sqrt{M}}\right)\gamma} \quad (\text{D-9})$$

This quantity is plotted as a function of  $\gamma$  in Figure 3b for several values of  $M$ . The results follow very closely the observed dependence of the Gaussian exponents shown in Figure 3a. As the number of surface elements increases, the quantity in eq D-9 becomes less sensitive to variations in  $\zeta$ , and in the limit  $M \rightarrow \infty$ , the scaled energy is exactly the Born solvation energy for any  $\gamma > 0$ .

## Appendix E

**Smooth Surface Area Model.** In this appendix a simple smooth surface area model is proposed based on a discretized solvent accessible surface and the smoothing scheme introduced in the main text. In particular a formula for the shift parameter  $\alpha$  is derived that shifts the center of the switching region relative to the atomic radius (Figure 2).

For a diatomic system consisting of atoms 1 and 2 on the  $z$  axis, consider the surface area of atom 2 that lies within the switching region of atom 1 ( $\widetilde{S}A_2$  in Figure 2); i.e., between the outer switching radius  $R_{\text{out}_1}$  and the atomic radius  $R_1$  (since the exact surface area does not penetrate  $R_1$ ). This region of surface area on atom 2 is

$$\widetilde{S}A_2 = 2\pi R_2^2 \int_{\theta_0}^{\theta_{\text{out}}} \sin(\theta) d\theta \quad (\text{E-1})$$

where integration is in spherical polar coordinates around atom 2, and  $\theta_0$  and  $\theta_{\text{out}}$  are given by

$$\theta_0 = \cos^{-1}(r_{12} + R_2^2 - R_1^2)/(2r_{12}R_2) \quad (\text{E-2})$$

$$\theta_{\text{out}} = \cos^{-1}(r_{12} + R_2^2 - R_{\text{out}_1}^2)/(2r_{12}R_2) \quad (\text{E-3})$$

The integral centered on atom 2 can be transformed into an integral centered on atom 1 that can be computed analytically,

$$\begin{aligned} \widetilde{S}A_2 &= 2\pi(R_2/r_{12}) \int_{R_1}^{R_{\text{out}_1}} r dr \\ &= \frac{(1 - \alpha_1)R_{\text{sw}_1} [(1 - \alpha_1) + 2R_1] \pi R_2}{r_{12}} \end{aligned} \quad (\text{E-4})$$

In the present model, the "surface area" is defined to include integration of the switching function in the switching region so that the surface area is a smooth function even for a discretized surface. This is desirable if one chooses to include empirical energy terms such as cavitation and dispersion terms that are functions of the surface area. The expression for the surface area of atom 2 in the present model is

$$\begin{aligned} \widetilde{S}A_2 &= 2\pi(R_2/r_{12}) \int_{R_{\text{in}_1}}^{R_{\text{out}_1}} S_{\text{wf}}[(r - R_{\text{in}_1})/R_{\text{sw}_1}] r dr \\ &= \frac{\pi R_2 R_{\text{sw}_1} \left[ R_1 + \left(\frac{5}{7} - \alpha\right) R_{\text{sw}_1} \right]}{r_{12}} \end{aligned} \quad (\text{E-5})$$

where  $S_{\text{wf}}(r)$  is the switching function defined in eq 64. If it is required that the surface area of eq E-5 equals the exact surface area of eq E-4 for a diatomic system, an equation is obtained that can be solved for the parameter  $\alpha$ . The result is

$$\alpha_1 = \frac{1}{2} + \frac{R_1}{R_{\text{sw}_1}} - \sqrt{\left(\frac{R_1}{R_{\text{sw}_1}}\right)^2 - \beta^2} = \frac{1}{2} + \frac{1}{\gamma} - \sqrt{\frac{1}{\gamma^2} - \beta^2} \quad (\text{E-6})$$

where (from eq 86)  $1/\gamma = R_1/R_{\text{sw}_1}$ , and  $\beta$  is a parameter that depends on the form of the switching function that in the present case (eq 64) is equal to  $(2\sqrt{7})^{-1}$ . Note that the parameter  $\alpha_1$  by this definition is independent of the radius  $R_2$  and separation distance  $R_{12}$  and hence can be evaluated uniquely for each atom (instead of each atom pair) and does not contribute to gradient terms. Although it is possible that one might derive an improved form for the  $\alpha$  parameters, for the present examples, this simple description is adequate and amenable to facile implementation and efficient calculation. Moreover, the importance of the  $\alpha$  parameters become less significant at higher surface discretization levels where the  $R_{\text{sw}}$  values become smaller. Consequently, increasing the discretization level allows a systematic means of obtaining a more accurate solution.

## References and Notes

- (1) Gilson, M. K. *Curr. Opin. Struct. Biol.* **1995**, *5*, 216–223.
- (2) Honig, B.; Nicholls, A. *Science* **1995**, *268*, 1144–1149.
- (3) Schaefer, M.; Karplus, M. *J. Phys. Chem.* **1995**, *100*, 1578–1599.
- (4) Smith, P. E.; Pettitt, B. M. *J. Phys. Chem.* **1994**, *98*, 9700–9711.
- (5) Perkyms, J.; Pettitt, B. M. *Biophys. Chem.* **1994**, *51*, 129–146.
- (6) Tomasi, J.; Persico, M. *Chem. Rev.* **1994**, *94*, 2027–2094.
- (7) Cramer, C. J.; Truhlar, D. G. *Reviews in Computational Chemistry*; VCH Publishers, Inc.: New York, **1995**; Vol. VI Continuum Solvation Models: Classical and Quantum Mechanical Implementations, Chapter 1, pp 1–73.

- (8) Tomasi, J.; Mennucci, B.; Cammi, R.; Cossi, M. *Computational Approaches to Biochemical Reactivity*; Kluwer Academic Publishers: Dordrecht, 1997; Chapter 1, pp 1–102.
- (9) Bashford, D.; Karplus, M. *Biochemistry* **1990**, *29*, 10219.
- (10) van Vlijmen, H. W. T.; Curry, S.; Schaefer, M.; Karplus, M. *J. Mol. Biol.* **1998**, *275*, 295–308.
- (11) Basilevsky, M. V.; Rostov, I. V.; Newton, M. D. *Chem. Phys.* **1998**, *232*, 189.
- (12) Lazaridis, T.; Karplus, M. *Science* **1997**, *278*, 1928–1931.
- (13) Schaefer, M.; Bartels, C.; Karplus, M. *J. Mol. Biol.* **1998**, *284*, 835–848.
- (14) Cossi, M.; Mennucci, B.; Cammi, R. *J. Comput. Chem.* **1996**, *17*, 57–73.
- (15) Klamt, A.; Schüürmann, G. *J. Chem. Soc., Perkin. Trans. 2* **1993**, 799–805.
- (16) Truong, T. N.; Stefanovich, E. V. *J. Chem. Phys.* **1995**, *103*, 3709–3717.
- (17) Pomelli, C. S.; Tomasi, J. *Theor. Chem. Acc.* **1997**, *96*, 39–43.
- (18) Barone, V.; Cossi, M.; Tomasi, J. *J. Comput. Chem.* **1998**, *19*, 404–417.
- (19) Jackson, J. D. *Classical Electrodynamics*; 2nd ed.; John Wiley & Sons: New York, 1975.
- (20) Gelfand, I. M.; Fomin, S. V. *Calculus of Variations*; Prentice-Hall, Inc.: Englewood Cliffs; New Jersey, 1963.
- (21) Zhou, Z.; Payne, P.; Vasquez, M.; Kuhn, N.; Levitt, M. *J. Comput. Chem.* **1996**, *11*, 1344–1351.
- (22) Truong, T. N.; Stefanovich, E. V. *Chem. Phys. Lett.* **1995**, *240*, 253–260.
- (23) Stefanovich, E. V.; Truong, T. N. *Chem. Phys. Lett.* **1995**, *244*, 65–74.
- (24) Truong, T. N.; Nguyen, U. N.; Stefanovich, E. V. *Int. J. Quantum Chem.: Quantum Chem. Sympos.* **30** **1996**, 403–410.
- (25) Stefanovich, E. V.; Truong, T. N. *J. Phys. Chem. B* **1998**, *102*, 3018–3022.
- (26) York, D. M.; Lee, T.-S.; Yang, W. *Chem. Phys. Lett.* **1996**, *263*, 297–304.
- (27) York, D. M.; Lee, T.-S.; Yang, W. *J. Am. Chem. Soc.* **1996**, *118*, 10940–10941.
- (28) Baldrige, K.; Klamt, A. *J. Chem. Phys.* **1997**, *106*, 6622–6633.
- (29) Klamt, A.; Jonas, V.; Bürger, T.; Lohrenz, J. C. W. *J. Phys. Chem. A* **1998**, *102*, 5074–5085.
- (30) Andzelm, J.; Kömel, C.; Klamt, A. *J. Chem. Phys.* **1995**, *103*, 9312–9320.
- (31) Barone, V.; Cossi, M. *J. Phys. Chem. A* **1998**, *102*, 1995–2001.
- (32) Press, W. H.; Teukolsky, S. A.; Vetterling, W. T.; Flannery, B. P. *Numerical Recipes in Fortran: The Art of Scientific Computing*, 2nd ed.; Cambridge University Press: New York, 1992.
- (33) York, D. M.; Lee, T.-S.; Yang, W. *Phys. Rev. Lett.* **1998**, *80*, 5011–5014.
- (34) York, D. M.; Yang, W. *J. Chem. Phys.* **1996**, *104*, 159–172.
- (35) Chipman, D. M. *J. Chem. Phys.* **1997**, *106*, 10194–10206.
- (36) Zhan, C.; Bentley, J.; Chipman, D. M. *J. Chem. Phys.* **1998**, *108*, 177–192.
- (37) Im, W.; Beglov, D.; Roux, B. *Comput. Phys. Commun.* **1998**, *111*, 59–75.
- (38) Cammi, R.; Tomasi, J. *J. Chem. Phys.* **1994**, *100*, 7495–7502.
- (39) Cammi, R.; Tomasi, J. *J. Chem. Phys.* **1994**, *101*, 3888–3897.
- (40) Cancès, E.; Mennucci, B. *J. Chem. Phys.* **1998**, *109*, 250–259.
- (41) Cancès, E.; Mennucci, B.; Tomasi, J. *J. Chem. Phys.* **1998**, *109*, 260–266.
- (42) Pulay, P. Calculation of forces by non-Hellmann–Feynman methods. *The Force Concept in Chemistry*; Van Nostrand Reinhold Co.: New York, 1981; Chapter 9, pp 444–480.
- (43) Delley, B. *J. Comput. Chem.* **1996**, *17*, 1152–1155.
- (44) Becke, A. D.; Dickson, R. M. *J. Chem. Phys.* **1988**, *89*, 2993.
- (45) Delley, B. *J. Chem. Phys.* **1990**, *92*, 508.
- (46) St-Amant, A. *Reviews in Computational Chemistry*; VCH Publishers, Inc: New York, 1996; Vol. VII (Density Functional Methods in Biomolecular Modeling), Chapter 5, pp 217–259.
- (47) Dunlap, B. I.; Connolly, J. W. D.; Sabin, J. R. *J. Chem. Phys.* **1979**, *71*, 3396.
- (48) Lee, T.-S.; York, D. M.; Yang, W. *J. Chem. Phys.* **1995**, *102*, 7549–7556.
- (49) Luty, B. A.; Davis, E.; McCammon, J. A. *J. Comput. Chem.* **1992**, *13*, 1114.
- (50) Lopez, X.; Dejaegere, A.; Karplus, M. *J. Am. Chem. Soc.* **1999**, *121*, 5548–5558.
- (51) Sridharan, S.; Nicholls, A.; Sharp, K. A. *J. Comput. Chem.* **1995**, *16*, 1038–1044.
- (52) Pomelli, C. S.; Tomasi, J. *Theor. Chem. Acc.* **1998**, *99*, 34–43.
- (53) Cramer, C. J.; Truhlar, D. G. *Science* **1992**, *256*, 213–217.
- (54) Stavrev, K. K.; Tamm, T.; Zerner, M. C. *Int. J. Quantum Chem.: Quantum Chem. Sympos.* **30** **1996**, 373–382.
- (55) Beglov, D.; Roux, B. *J. Chem. Phys.* **1994**, *100*, 9050–9063.
- (56) A function is said to be “smooth” with respect to a variable if the corresponding first derivative is continuous.
- (57) The theoretical value  $\Sigma$  for the integrated polarization surface charge is given by eq 21 and depends on the integrated static charge inside the cavity. Sometimes it is desirable to instead set  $\Sigma$  equal to the integrated polarization density given in eq 14. In this way an effective polarization surface charge is generated that is normalized to the total polarization charge and has the additional advantage that the normalization factor is independent of geometry (unlike  $Q_0(V_1)$ ).
- (58) The constant chemical potential  $\mu = [\partial E/\partial \rho]_{\rho_0}$  derives from the constrained variational condition for the total energy:  $\delta \{E[\rho] - \mu \int \rho d^3r\} = 0$ .
- (59) The solvation energy is minimized with respect to variations in the surface charge density that is expanded in the basis of surface elements. Appearance of new surface elements causes a discontinuous increase in the variational basis space that can only decrease (or have no effect on) the solvation energy.
- (60) For two uniformly charged spherical reactants with radii  $R_1$  and  $R_2$  and charges  $q_1$  and  $q_2$  that react to form a uniformly charged spherical transition state with the same volume (i.e., radius  $R = (R_1^3 + R_2^3)^{1/3}$ ), the ratio of the solvation energy of the transition state  $E_{ts}$  and of the infinitely separated reactants  $E_r$  is given by  $E_{ts}/E_r = [(q_1 + q_2)^2/R]/(q_1^2/R_1 + q_2^2/R_2)$ . For reactants of equal size, the ratio is (1) for  $q_1 = q_2 \neq 0$ ,  $E_{ts}/E_r = 2^{2/3} \sim 1.6$ , 2) for  $q_1 \neq q_2 = 0$ ,  $E_{ts}/E_r = 2^{-1/3} \sim 0.8$ , and 3) for  $q_1 = -q_2 \neq 0$ ,  $E_{ts}/E_r = 0$ . A ratio greater than 1 indicates preferential solvent stabilization of the transition state, a ratio less than 1 indicates the reverse.
- (61) The solvent accessible surface is equivalent to the van der Waals surface with radii increased by the probe radius, and the van der Waals surface is identical to the solvent accessible surface with zero probe radius.
- (62) In the case of the conductor-like screening model, the number of surface elements representing the polarization surface charge determines the dimensions of the vectors and matrices in eqs 39–43. The situation is directly analogous in all boundary element methods.